PROxAb Shuttle: A non-covalent plug-and-play platform for the rapid generation of tumor-targeting antibody-PROTAC conjugates

Hendrik Schneider[a], Sebastian Jäger[a], Doreen Könning[a], Nicolas Rasche[a], Christian Schröter[a], Desislava Elter[a], Andreas Evers[a], Marc Lecomte[a], Federico Riccardi Sirtori[b], Daniel Schwarz[a], Ansgar Wegener[a], Ingo Hartung[a] and Marcel Rieker*[a]

[a]Merck KGaA, Darmstadt, Germany; Frankfurter Strasse 250, 64293 Darmstadt, Germany
[b]Merck KGaA, RBM S.p.A., Via Ribes 1, 10010 Colleretto Giacosa (TO), Italy

*Corresponding Author: marcel.rieker@merckgroup.com

Abstract: Proteolysis-targeting chimeras (PROTACs) have evolved in recent years from an academic idea to a therapeutic modality with more than 25 active clinical programs. However, achieving oral bioavailability and cell-type specificity remains a challenge, especially for PROTACs recruiting the von Hippel-Lindau (VHL) E3 ligase. Herein, we present an unprecedented, plug-and-play platform for VHL-recruiting PROTACs to overcome these limitations. Our platform allows for the generation of non-covalent antibody-PROTAC complexes within minutes and obviates the need for prior PROTAC modification, antibody-drug linker chemistry optimization or bioconjugation. Our technology relies on camelid-derived antibody domains (VHHs) which can easily be engineered into existing therapeutic antibody scaffolds. The resulting targeted, bispecific fusion proteins can be complexed with PROTACs at defined PROTAC-to-antibody ratios and have been termed PROxAb Shuttles. PROxAb Shuttles can prolong the half-life of PROTACs from hours to days, demonstrate anti-tumor efficacy *in vivo* and have the potential for reloading *in vivo* to further boost efficacy.

Introduction

Targeted Protein Degradation (TPD) has attracted major interest from both academia and industry over the past years since it enables the selective knockdown of disease-causing proteins with the well-established drug modality of small molecules. The field has been fueled by the more than 25 novel degraders that have advanced into clinical trials within the last 5 years. Degrader modalities have taken various designs, with one of the most established entity being proteolysis-targeting chimeras, or PROTACs, which leverage the ubiquitin-proteasome pathway to degrade and remove disease-causing proteins.[1,2] The inherent advantage of PROTACs lies, among others, in their ability to degrade proteins which have been difficult to address by conventional inhibitors due to the lack of a druggable functional binding pocket. In addition, degrader molecules exhibit a catalytic mode of action that allows strong cellular activity resulting from low compound concentrations. For proteins with slow resynthesis rates, functional effects induced by PROTACs can continue after the PROTAC has already been cleared from the system. The most advanced PROTACs in clinical development are ARV110 and ARV471, which target the androgen and estrogen receptor, respectively and are developed by the company Arvinas.

PROTACs are heterobifunctional molecules that consist of a protein-targeting subunit, a moiety that recruits the respective E3 ligase, and a chemical linker which interconnects both units (Figure 1A). The two E3 ligases most often leveraged for the design of PROTACs are Cereblon (CRBN) and von Hippel-Lindau tumor suppressor (VHL), both belonging to the family of culin ring ligase (CRL) E3 complexes.[3] Although most PROTACs are highly efficient, they are generally not tissue-specific by nature as they exploit VHL and CRBN E3 ligases with broad expression profiles. Tissue-specific degradation of target proteins may be beneficial for minimizing side effects (especially when targeting wild-type proteins), however, functional PROTACs exploiting E3 ligases with restricted tissue distribution are difficult to identify and the development of novel E3 ligase ligands remains a significant challenge.[4] In addition, PROTAC development and efficacy are often hampered by their short half-life *in vivo*[5,6] and low cellular permeability[7], limiting their ability to enter cells and induce protein degradation. The larger size of these chimeric molecules when compared to conventional inhibitors negatively impacts oral bioavailability, solubility, and the absorption, distribution, metabolism and excretion (ADME) properties[8], especially for VHL-targeting PROTACs, due to the peptidic nature of available VHL ligands.[9] Therefore, targeted delivery of PROTACs has evolved as a way to enhance specificity and address the aforementioned liabilities. To this end, covalent conjugation of a PROTAC to an antibody has emerged as an innovative approach that builds on the success of Antibody-Drug Conjugates (ADCs).[10] ADCs rely on the targeted delivery of cytotoxic drugs and have been explored in the clinic for decades, with overall 13 ADCs being approved up to now.[11] The resulting antibody-PROTAC conjugates combine the cellular specificity and favorable pharmacokinetic (PK) profile of the antibody with the protein-degrading ability of the attached PROTAC. While some publications have outlined different strategies for covalent conjugation of the chimeric degrader modality to the antibody, the heterobifunctional nature of PROTACs often impairs the attachment of an additional linker in a suitable exit vector (Figure 1B).[8,10,12] Adding an attachment point to the already bifunctional PROTAC molecule further increases chemical complexity and provides a risk for negatively impacting the biological function of the PROTAC.[8]

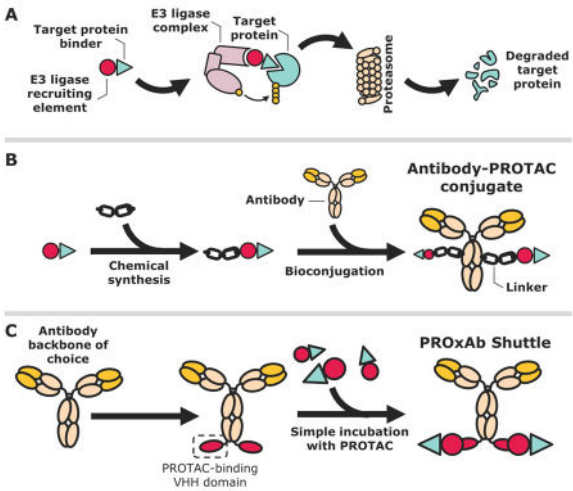

Figure 1. Comparison of the non-covalent PROxAb Shuttle technology with covalent antibody-PROTAC conjugates. A) Mode of action of Proteolysis-targeting chimeras (PROTACs). B) The covalent attachment of a PROTAC to an antibody relies on the identification of a suitable exit vector on the PROTAC for linker attachment. Subsequently, a respective linker-PROTAC molecule needs to be conjugated to the antibody backbone. C) PROxAb Shuttles rely on single domain antibodies derived from camelids which engage the VHL ligand-binding subunit of PROTACs. By fusing such an antibody domain to existing antibody scaffolds, bispecific fusion proteins are obtained.

Recently, alternative TPD modalities that encompass antibodies and membrane-bound E3 ligases have been described. Towards this end, Marei and coworkers generated bispecific, proteolysis-targeting antibodies called PROTABs

which bind to a membrane-localized ubiquitin E3 ligase that is selectively expressed in colorectal cancer, as well as to a transmembrane receptor.[13] In addition, the targeted delivery of PROTACs into tumor tissue has also been achieved by fusing the PROTAC to suitable receptor ligands, such as folate. Liu and colleagues could show that fusing a folate moiety to a PROTAC enables the selective delivery of the PROTAC to folate receptor-positive tumor cells.[14] Specific tumor-targeting of PROTACs has also been achieved by chemical conjugation of the degrader to nucleolus-targeting aptamers[15] or amphiphilic diblock copolymers, resulting in self-assembling, micellar nanoparticles.[16] The present work describes a novel TPD platform that involves the non-covalent complexation of PROTACs by bispecific antibodies. This technology leverages single-domain antibodies derived from camelids which bind to the E3 ligase-recruiting subunit of the PROTAC and can be fused to existing therapeutic antibody scaffolds (Figure 1C). The approach relies on the concept of non-covalent interactions between an antibody and a small molecule, similar to previously published approaches by Gupta et al. for the generation of ADCs and several publications authored by scientists at Roche that involve non-covalent binding of small molecules such as biotin or digoxigenin by an antibody.[17–19] Non-covalent approaches have, for instance, been employed for the selective delivery of cytotoxic agents, such as DNA damaging agents, however, the majority of these concepts still relies on the chemical modification of the small molecule with a hapten that is then bound by the antibody.[20] Our platform technology, on the other hand, utilizes the heavy chain-only antibody domains from camelids (termed VHH domains or nanobodies) which directly interact with the VHL-binding portion of the PROTAC.[21] This approach omits the need for the attachment of haptens to the PROTAC and facilitates the generation of non-covalent antibody-PROTAC conjugates.

Camelid-derived single domain antibodies comprise an elongated complimentary determining region 3 (CDR3) and are able to access cryptic or hidden epitopes intractable for conventional antibodies.[22] It has indeed been shown that the elongated CDR3 loop of camelid VHH domains is able to adopt protruding and complex secondary structures that facilitate the interaction with recessed epitopes. As a consequence, VHH domains have been explored for a variety of different targets, including small molecules, and their development culminated in the FDA approval of caplacizumab for the treatment of thrombotic thrombocytopenic purpura (TTP) in 2019.[23] Owing to their small size, VHH domains can also easily be fused to therapeutic antibodies, yielding bispecific and multivalent entities.[24] Our team has generated VHH domains which engage the VHL ligase-recruiting portion of PROTACs. We have fused these domains to the *C*-terminus of therapeutic antibody scaffolds and could show that the resulting fusion proteins, termed PROxAb Shuttles, are able to form stable complexes with PROTACs. Precisely, PROxAb Shuttles non-covalently bind the unmodified PROTAC and the specificity of one VHH allows universal binding to a broad spectrum of different VHL-based PROTACs. Our non-covalent platform enables the rapid complexation of VHL-based PROTACs to antibodies and offers researchers and drug developers a 'plug-and-play' approach for the generation of antibody-PROTAC modalities within minutes. Moreover, PROxAb Shuttles are able to drastically prolong the half-life of the PROTAC *in vivo* compared to free PROTAC alone. In addition, PROxAb Shuttles offer the possibility of PROTAC re-loading by re-dosing of the free degrader to further prolong the anti-tumor effect *in vivo*. The technology comes with the benefit of limited synthesis effort as no linker chemistry or bioconjugation techniques are required to generate the resulting PROxAb Shuttle complexes and, as such, the biological function of the degrader is not influenced. The therapeutic antibody of choice needs to be modified only once with the VHL ligand-binding VHH domain and can subsequently be combined with a plethora of different VHL-based degraders in a modular approach. Ultimately, the technology has the potential to improve the therapeutic window of PROTACs that may be too toxic as a standalone therapy, enhance their efficacy by increasing their cell permeability and to improve the *in vivo* PK profile of PROTACs suffering from short half-lives. To the best of our knowledge, this is the first report of non-covalent, PROTAC-binding antibodies to date.

Results and Discussion

Anti-VHL ligand antibody domains can be used to convert therapeutic antibody scaffolds into bispecific PROTAC binders (PROxAb Shuttles).

For the generation of anti-VHL ligand antibodies, New World Camelids were immunized with different VH032-haptens (**1**-**4**) conjugated to immunogenic carrier proteins (Figure 2 and Supplementary Information). Of note, VH032 (**5**) is the E3 ligase-engaging structure found in VHL-recruiting PROTACs (Figure 3 and Figure S1). After immunization, titers were determined using enzyme-linked immunosorbent assays (ELISA) and blood samples of camelids were drawn after sufficient titers were achieved. After the isolation of mRNA encoding for the desired VHH domains from peripheral blood mononuclear cells (PBMCs) and translation into cDNA, an antibody phage display library was generated and screened for binding to the VHL-hapten conjugates.

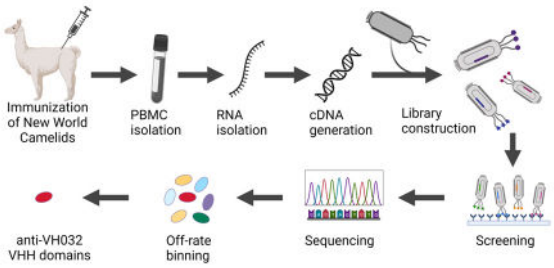

Figure 2. Schematic depiction of the workflow for the generation of VHL ligand-specific antibody domains. Figure created with BioRender.com.

Ultimately, 113 unique antibody clones were identified from the camelid immune library. Prior to reformatting and recombinant expression, monoclonal VHH-displaying phages in bacterial supernatant were subjected to an off-rate screening using Bio-Layer Interferometry (BLI) to identify the most suitable VHH variants for non-covalent delivery with the longest off-rates (Figure S2). Selected VHH domains (termed Monovalent Immobilizer of Chimeras, or MICs) were genetically fused to the *C*-terminus of the antibody scaffold of the therapeutically used anti-CD33 antibody-drug conjugate gemtuzumab ozogamicin (αCD33xMIC) as well as an antibody scaffold that comprised the variable regions of the therapeutic anti-EGFR antibody cetuximab (αEGFRxMIC). The VHH domains and the antibody heavy chains were separated by a short glycine-serine linker. Subsequently, the reformatted fusion proteins were recombinantly expressed in human embryonic kidney (HEK) cells and purified from the cell medium after cellular secretion.

Expression levels and purity of the fusion proteins were comparable to those of the respective antibodies, indicating no negative impact by the fusion of the VHH domains. Next, surface plasmon resonance (SPR) was used to determine the affinity of the VHH-portion of the immobilized fusion proteins towards several VH032-based PROTACs in solution. We selected a broad range of different VH032-based PROTACs comprising aliphatic-, propanediol- and polyethylene glycol (PEG)-based linkers to ensure a certain variability with regard to linker exit vectors and functional groups within the PROTAC (Figure S3). Ultimately, we were able to identify MIC7 as the VHH domain with the highest affinity while accepting a broad diversity of VH032-based PROTACs. As depicted in Tables 1 and S1, MIC7 was able to bind almost all tested PROTACs with linker positions in R1 and R2 with single-digit nano- to subnanomolar affinities (Figure 3).

Table 1. Affinities of reformatted MIC7-based PROxAb Shuttles towards different PROTACs. The MIC7 domain was fused *C*-terminally to the heavy chains of gemtuzumab- and cetuximab-based antibody scaffolds. * = inactive diastereomer of cMET degrader.

PROTAC	Exit	VH032 substitution	K_D [M] of αCD33x MIC7	K_D [M] of αEGFRx MIC7
6 (GNE987)	R1	-	<1 X 10^{-9}	<1 X 10^{-9}
7 (GNE987P)	R1	-	2.0 X 10^{-9}	<1 X 10^{-9}
8 (ARV771)	R1	R4=Me	1.1 X 10^{-9}	5.4 X 10^{-9}
9 (BETTY2)	R1	-	2.1 X 10^{-9}	1.1 X 10^{-9}
10 (BETTY3)	R1	R3=OH	3.3 X 10^{-9}	1.9 X 10^{-9}
11 (cMETd1)	R1	R5=H, R6=OH*	1.2 X 10^{-8}	9.4 X 10^{-9}
12 (AT1)	R2	R1=Acyl	2.1 X 10^{-9}	1.2 X 10^{-9}
13 (SIM1)	R1	-	4.8 X 10^{-9}	1.9 X 10^{-9}
14 (SIAIS178)	R1	-	8.3 X 10^{-9}	<1 X 10^{-9}

Only one of the tested PROTACs (cMETd1) showed limited binding to MIC7, which was not surprising considering that the hydroxyl group of cMETd1 is present in (*S*)- and not (*R*)-configuration which reduces its ability to engage with VHL and MIC7.

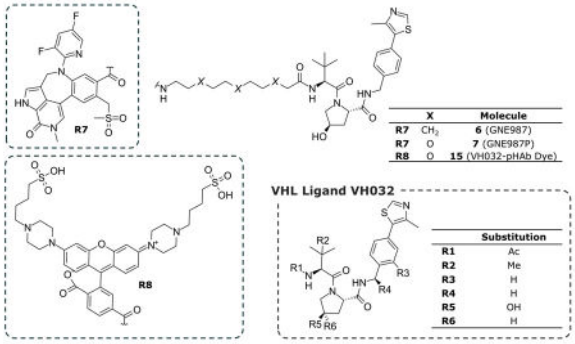

Figure 3. Overview of chemical structures of the PROTACs and tool compounds utilized in the scope of this work.

Generation of complexed PROxAb Shuttles.

We next aimed at investigating the optimal complexation procedure for the generation of PROxAb Shuttles with defined PROTAC-to-antibody ratios. Towards this end, the reformatted, anti-CD33 PROxAb Shuttle comprising the MIC7 VHH domain was incubated with the PROTAC GNE987 (**6**) at room temperature and at a ratio of 2:1 between PROTAC and antibody. GNE987 (**6**) targets the intracellular bromodomain-containing protein 4 (BRD4) and is bound with high affinity by the MIC7 VHH domain (Table 1).[5] The formation of PROxAb Shuttle complexes could already be observed within minutes and successful loading of the PROxAb Shuttle was confirmed by native size exclusion chromatography (SEC) coupled with native mass spectrometry (MS). As depicted in Figure 4A, the complexed and non-complexed αCD33xMIC7 Shuttles with a PROTAC-to-antibody ratio of 1.9 and 0, respectively, could be identified. Upon using native SEC coupled with native MS, it was possible to verify the loading of PROxAb Shuttles with defined PROTAC-to-antibody ratios. In addition, isothermal titration calorimetry (ITC) was used to determine the stoichiometry of the antibody/VH032 interaction, as depicted in Figure 4B which shows the binding isotherm for αCD33xMIC7 complexed with VH032. In this experiment, we observed symmetrical isotherms and interactions which were dominated by binding enthalpy. The binding is saturating at an apparent molar ratio of ~0.5, which is equivalent to a stoichiometry of N = 2.1. These results are in line with the expected ratio of two VH032 molecules binding to one PROxAb Shuttle comprising two MIC7 VHH entities. The symmetrical isotherm depicted in Figure 4B indicates a homogeneous binding process with one set of identical and independent binding sites.

PROxAb Shuttles efficiently internalize into cells and exhibit nanomolar potencies *in vitro*.

To assess whether the cellular binding of our PROxAb Shuttles was impaired by the fusion of the MIC7 VHH domain, cell lines with varying CD33 receptor expression were incubated with either unmodified antibody, PROTAC-complexed αCD33xMIC7 PROxAb Shuttle, or an isotype control for 45 minutes. An antibody targeting digoxigenin, which was likewise fused to MIC7 at its *C*-terminus, served as isotype control (αDIGxMIC7). Following the incubation, the cells were stained with a fluorescently labeled anti-human Fc detection antibody and subjected to flow cytometric analyses. The resulting mean fluorescence intensity (MFI) values for the MIC7-based PROxAb Shuttles, complexed or non-complexed with GNE987 (**6**), were compared to the parental αCD33 antibody and are depicted in Figure 5A, demonstrating that the fusion of the MIC7 VHH domain did not impair binding to CD33.

To gain further insights into the route of internalization of the PROxAb Shuttle, we synthesized a VH032 subunit that was linked to a pH-responsive dye (VH032-pHAb dye (**15**); Figure 3) via a PEG-based linker. The shift in environmental pH that occurs upon transition of the PROxAb Shuttle-bound VH032-pHAb dye (**15**) into the acidic environment of the endosomal and lysosomal vesicles causes an increase in the fluorescence signal. After incubation of CD33-positive cells with VH032-pHAb-complexed αCD33xMIC7 PROxAb Shuttle, the cells were subjected to flow cytometric analyses. As depicted in Figure 5B, the MFI values increased when cells were incubated with the PROxAb Shuttle complex in comparison to the corresponding VH032-pHAb dye-only control (**15**), demonstrating internalization of the Shuttle and accumulation of the VH032-pHAb dye (**15**) in the endolysosomal vesicles.

In order to show that PROTAC which is internalized via the PROxAb Shuttle also reaches its intracellular target, we next measured the degradation of BRD4 after incubation of CD33-positive MV4-11 cells with decreasing concentrations of GNE987-complexed αCD33xMIC7 and αDIGxMIC7 PROxAb Shuttles or GNE987 PROTAC (**6**) alone (Figure 5C). Following the incubation, cells were lysed at different time points and the cell lysates were subjected to Western Blot analyses to determine the remaining levels of BRD4 (Figure S4). Figure 5C shows the quantified BRD4 signal from the Western Blots in % and normalized to the solvent-only control. Upon incubation of the cells with the PROxAb Shuttles, a concentration-dependent decrease of the intracellular BRD4 signal could be observed for the αCD33xMIC7 Shuttle and for free PROTAC, whereas BRD4 signals were not impacted by the isotype control. These results demonstrate that the PROTAC, when delivered with a PROxAb Shuttle, can escape the lysosomal compartment to exert its intended mode of action. Moreover, these data demonstrate the stability of the PROxAb Shuttle complex under the assay conditions since the isotype control did not elicit BRD4 degradation. Notably, complete BRD4 degradation was achieved by the αCD33xMIC7 Shuttle at a concentration as low as 1 nM. Ultimately, we investigated whether it is possible to deliver PROTAC concentrations into tumor cells via the PROxAb Shuttle that are sufficient to elicit the intended pharmacological effect of cell killing. Since the PROxAb Shuttle complexes can be freshly prepared prior to each potency assay without any further purification step, we first performed titration experiments with different PROTAC-to-antibody ratios on target-negative cell lines (data not shown). This served to determine the ratio which would yield the lowest background signal to enable an accurate assessment of the median inhibitory concentrations of our PROxAb Shuttles in subsequent experiments. Ultimately, a PROTAC-to-antibody ratio of 1 was selected for the *in vitro* potency assays. Finally, CD33- and EGFR-targeting PROxAb Shuttles were incubated with either, CD33- or EGFR-positive and negative tumor cell lines with varying receptor expression. The αDIGxMIC7 PROxAb Shuttle served as isotype control and free PROTAC was included as a positive control. Figure 5D depicts the

resulting dose-response curves for each individual cell line and for each PROxAb Shuttle with a PROTAC-to-antibody ratio of 1. The complexed αCD33xMIC7 and αEGFRxMIC7 Shuttles exhibited potencies on target positive cells in the nanomolar range and were able to selectively deliver cytotoxic concentrations of PROTACs to the desired cells (Table S2). Notably, the cytotoxicity of each Shuttle was also dependent on the number of target receptors on the cell surface. Whereas the EGFR copy numbers are high and in the range of several hundred thousand for the tested A431 and MDA-MB-468 cells,[25] the CD33-positive cell lines MV4-11 and MOLM13 comprise a lower receptor number of

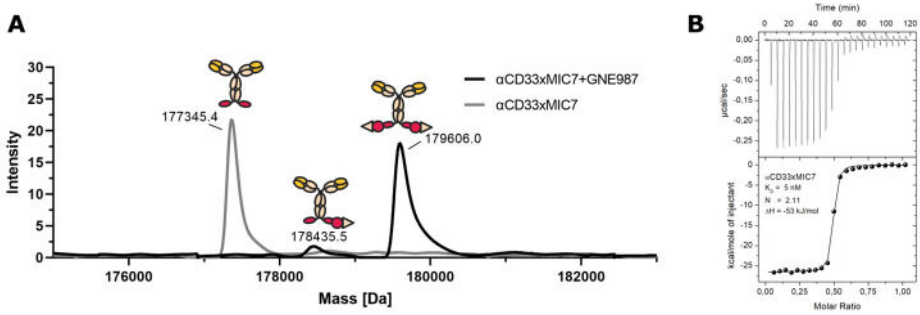

Figure 4. Complexation process and stoichiometry of the antibody/PROTAC interaction. A) Spectrum of native SEC/native MS measurements for the αCD33xMIC7 PROxAb Shuttle complexation reaction with the PROTAC GNE987 (**6**). Distinct peaks for the PROxAb Shuttles with a PROTAC-to-antibody ratio of 0 and 2 can be identified, respectively. B) Binding isotherm of the αCD33xMIC7 PROxAb Shuttle with the VHL ligand VH032 (**5**).

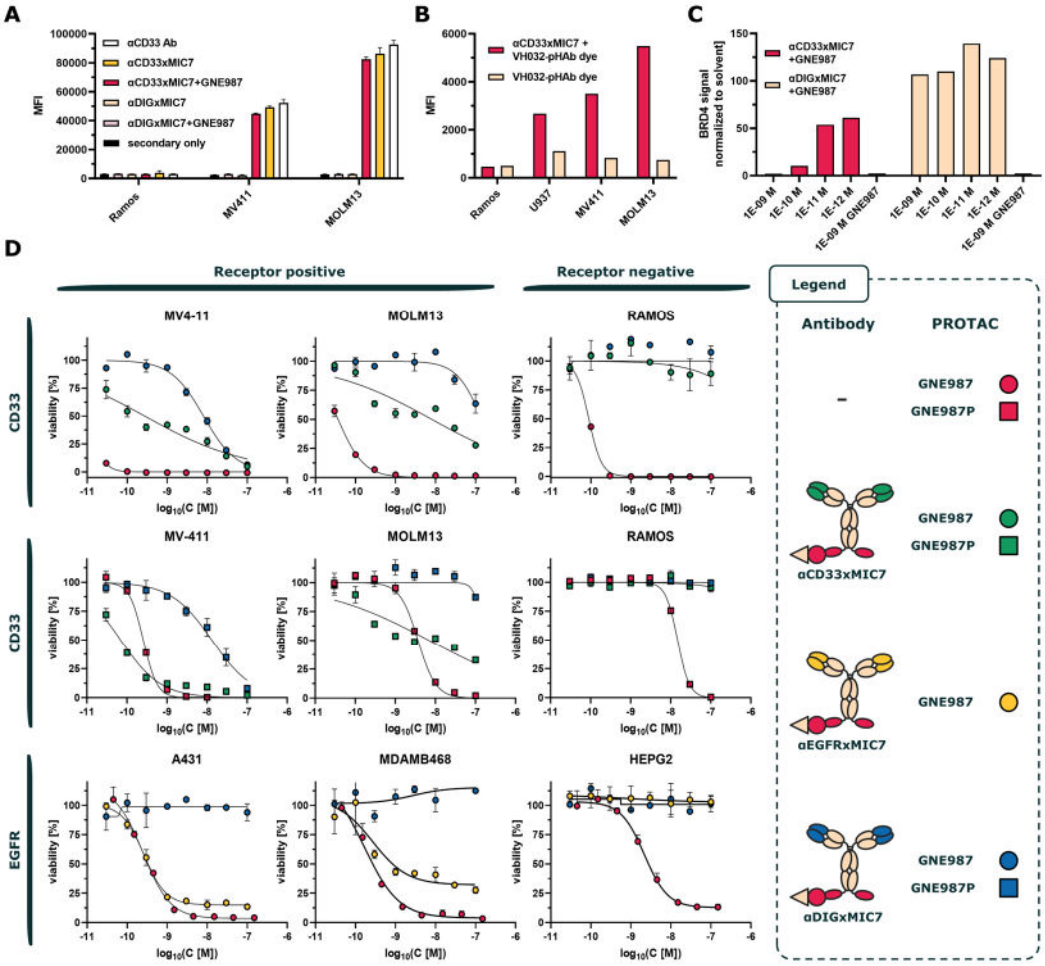

Figure 5. *In vitro* characterization of MIC7-based PROxAb Shuttles. A) Cell binding of anti-CD33 antibody scaffolds with and without a *C*-terminally fused MIC7 antibody domain to CD33 positive cells. PROxAb Shuttles were tested in the complexed (PROTAC-to-antibody ratio = 1) and non-complexed form with GNE987 PROTAC (**6**). Bars represent the average of technical duplicates. Ab = antibody. B) Flow cytometric analysis of the internalization of the αCD33xMIC7 PROxAb Shuttle complexed with VH032-pHAb dye (**15**) over a period of 24 hours (dye-to-antibody ratio = 1) compared to free dye alone on different CD33-expressing cell lines. C) Western Blot analysis and quantification of BRD4 levels in CD33-positive cells treated with different concentrations of αCD33xMIC7 PROxAb Shuttle complexed with GNE987 or free GNE987 (**6**) at a PROTAC-to-antibody ratio of 1. The intensity of individual Western Blot signals was normalized to the loading control (Actin; Figure S4). D) Cell viability assays of complexed αCD33- and αEGFRxMIC7 PROxAb Shuttles with different PROTACs on target-positive and target-negative cell lines at PROTAC-to-antibody ratios of 1. Compounds were incubated on cells for overall 72 hours. An αDIGxMIC7 Shuttle was included as an isotype control and free PROTAC was used as the positive control for each assay. Upper panel: Dose-response curves of αCD33xMIC7 Shuttles and isotype control complexed with GNE987(**6**). Middle panel: Dose-response curves of αCD33xMIC7 PROxAb Shuttle and isotype control complexed with GNE987P (**7**). Lower panel: Dose-response curves of αEGFRxMIC7 PROxAb Shuttle and isotype control complexed with GNE987 (**6**). Sigmoidal curves represent the mean of technical duplicates.

around 18,000 to 48,000 copies.[26,27] These differences are reflected in the higher half maximal inhibitory concentration (IC_{50}) values of the GNE987-complexed αCD33xMIC7 Shuttle when compared to free PROTAC alone (Figure 5D, upper panel), while the complexed aEGFRxMIC7 Shuttle shows a similar potency in comparison to the free PROTAC. In addition to GNE987 (**6**), we also complexed the αCD33xMIC7 Shuttle with the more hydrophilic variant of GNE987(**6**), termed GNE987P (**7**).[12] Combining a more hydrophilic and, therefore, less cell permeable PROTAC such as GNE987P (**7**) with the PROxAb Shuttle technology should enable to boost PROTAC potency due to a facilitated active delivery into the target cell. As can be seen in the middle panel of Figure 5B and in Table S2, GNE987P (**7**) in complex with our αCD33xMIC7 Shuttle was more efficacious when compared to the free PROTAC alone, particularly on MV4-11 cells. Importantly, no cytotoxic effects were observed for all targeted PROxAb Shuttles on either, the CD33- or EGFR-negative cell lines regardless of the complexed PROTAC. After these initial experiments, we were able to demonstrate similar effects for numerous PROxAb Shuttles based on different therapeutic antibody scaffolds, also in combination with other PROTACs than GNE987 (**6**) and GNE987P (**7**), which further emphasizes the platform potential of PROxAb Shuttles (Table S3).

PROxAb Shuttles can extend the half-life of PROTACs from hours to days.

After demonstrating that PROxAb Shuttles effectively deliver VHL-based PROTACs *in vitro*, we next investigated their pharmacokinetic (PK) profile in C57BL/6N mice. In order to show that the overall PK of the antibodies was not altered by the VHH fusion, we first compared the PK parameters of the unmodified αCD33 antibody with 2 different αCD33 PROxAb Shuttles without complexed PROTAC (Figure 6A). Besides the MIC7 Shuttle, a second αCD33 PROxAb Shuttle comprising the VHL-binding VHH domain MIC5 was included as well (αCD33xMIC5) in order to assess the influence of different antibody off-rates on the pharmacokinetics of the complexed PROTAC in further experiments. MIC5 exhibits a lower affinity towards VH032-based PROTACs as well as a faster off-rate when compared to MIC7, as assessed in previous surface plasmon resonance experiments (Table S4). Table 2 summarizes the pharmacokinetic parameters for the respective antibodies at an administered dose of 30 mg/kg. All tested antibody variants exhibited half-lives of approximately 10 days, emphasizing that the PK profile of the αCD33 antibody is not influenced by the *C*-terminal fusion of the MIC5 and MIC7 VHH domains. Moving forward, we evaluated the αCD33xMIC7 and αCD33xMIC5 Shuttles with and without bound PROTAC in order to confirm that the associated PROTAC does not influence the PK property of the fusion protein. In contrast to previous *in vitro* assays, the PROTAC-to-antibody ratio was set to 2 for all *in vivo* experiments to reach a higher complexed PROTAC exposure and, therefore, to increase the efficacy of the Shuttles. Figure 6B shows that the total antibody concentration profile in plasma as assessed *via* electrochemiluminescence immunoassay, is nearly identical for the complexed and non-complexed αCD33 PROxAb Shuttles, indicating a similar PK profile for the antibody.

Next, we investigated the influence of the PROxAb Shuttle on the half-life of the PROTAC. To achieve this, C57BL/6N mice were dosed with either 30 mg/kg of GNE987-complexed αCD33xMIC7 and αCD33xMIC5 Shuttles (comprising overall 0.38 mg/kg of GNE987 **(6)**) or a dose of 0.3 mg/kg of GNE987 alone (**6**). As can be seen in Figure 6C, the half-life of GNE987 (**6**) dosed alone was approximately 2 hours and could be drastically prolonged to more than 4 days (105 hours) when complexed by the αCD33xMIC7 Shuttle. Interestingly, the half-life of GNE987 (**6**) when complexed by the MIC5-based PROxAb Shuttle could solely be increased up to 30 hours, indicating that affinity is playing a role for efficient and long-lasting capture of the PROTAC *in vivo*. The difference in affinity between MIC5 and MIC7 for GNE987 (**6**), as measured via surface plasmon resonance, was almost 17-fold and translated into a 3.5-fold higher PROTAC half-life in mice. Notably, the off-rates (k_{off}) of both antibody domains varied by a factor of 21, while the on-rates (k_{on}) were in the same range (Table S4). Fine-tuning of the antibody/PROTAC affinity by, for instance, affinity maturation of MIC7 with a focus on dedicated off-rate screenings may result in even tighter interactions and even longer PROTAC *in vivo* half-lives. It is worth noticing that the MIC5 and the MIC7-based αCD33 PROxAb Shuttle complexes were well-tolerated in treated mice, and no loss of body weight or any clinical signs of toxicity were observed (data not shown).

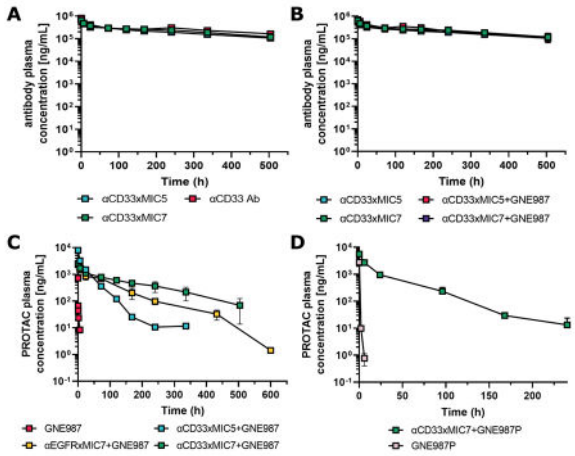

Figure 6. Pharmacokinetic profiles of complexed (PROTAC-to-antibody ratio of 2) and non-complexed PROxAb Shuttles (30 mg/kg; i.v. route) with GNE987 (**6**) (0.3 mg/kg) in mice. A) Comparison of the total antibody concentration profiles of unmodified αCD33 antibody scaffold with non-complexed αCD33xMIC7 and αCD33xMIC5 PROxAb Shuttles. B) Total antibody concentration profiles of complexed and non-complexed αCD33xMIC7 and αCD33xMIC5 PROxAb Shuttle variants. C) Total PROTAC profiles of αCD33xMIC7, αCD33xMIC5 and αEGFRxMIC7 Shuttles after complexation with GNE987 (**6**), as well as free GNE987 (**6**). D) Total PROTAC profiles of the αCD33xMIC7 PROxAb Shuttle after complexation with GNE987P (**7**), as well as free GNE987P (**7**).

Building on these findings, we next investigated the PK properties of the αEGFRxMIC7 Shuttle in order to extend our previous analyses to another antibody scaffolds. Similar to the results obtained for the αCD33 Shuttle variants, the αEGFRxMIC7 PROxAb Shuttle was able to prolong the *in vivo* half-life of GNE987 (**6**) from 2 hours to approximately 66 hours as compared to the PROTAC alone (Figure 6C).

To further demonstrate the versatility of the PROxAb Shuttle technology with regards to the PROTAC, we ultimately thought to investigate the combination of αCD33xMIC7 PROxAb Shuttles with another PROTAC than GNE987 (**6**). For this purpose, the αCD33xMIC7 Shuttle was complexed with GNE987P (**7**) at a PROTAC-to-antibody ratio of 2 and administered at 30 mg/kg (comprising overall 0.38 mg/kg of GNE987P (7)) while a second cohort was dosed with 0.3 mg/kg of GNE98P alone (**7**) (Figure 6D). In this case, the half-life of GNE987P (**7**) could be increased from 0.5 to 33.6 hours, i.e. a factor of >60-fold. These results further validate the *in vivo* half-life-prolongation effect of the PROTAC that is achievable by the PROxAb Shuttle concept.

Leveraging a non-covalent rather than a covalent bond between the antibody and the PROTAC has the advantage of potential re-binding to the antibody. This means, that PROTACs which may be released from the Shuttle in circulation can in fact be re-bound by the antibody. Fine-tuning of the antibody/PROTAC interaction by additional protein engineering may result in tailor-made 'PROTAC reservoirs' that could balance out suboptimal plasma stability by slow release from the Shuttle.[28] In fact, multiple non-covalent interactions can even surpass a single covalent bond with regards to affinity and form an almost irreversible connection.[17]

Table 2. Pharmacokinetic parameters for different PROTACs, antibodies and either complexed or non-complexed PROxAb Shuttles with PROTAC-to-antibody ratios of 2. Abbreviations: $t_{1/2}$ = half-life time; Cl = clearance, Vss = volume of distribution at steady-state; TAb = total antibody.

Molecule	Analyte	$t_{1/2}$ [h]	C_{max} [ng/mL]	$AUC_{0\text{-}inf}$ [h x ng/mL]	Cl [mL/h/kg]	Vss [mL/kg]
6 (GNE987)	PROTAC	2.2	7.2×10^2	3.5×10^2	850	1348
7 (GNE987P)	PROTAC	0.54	2.8×10^3	1.3×10^3	236	86
αCD33 antibody	TAb	237	8.1×10^5	2.2×10^8	0.14	74
αCD33xMIC5	TAb	351	6.6×10^5	1.7×10^8	0.22	85
αCD33xMIC5 with **6**	PROTAC	30	7.9×10^3	1.3×10^5	3.0	100
αCD33xMIC5 with **6**	TAb	276	7.2×10^5	1.7×10^8	0.18	67
αCD33xMIC7	TAb	274	6.8×10^5	1.6×10^8	0.19	75
αCD33xMIC7 with **6**	PROTAC	105	2.5×10^3	2.3×10^5	1.74	270
αCD33xMIC7 with **6**	TAb	304	5.9×10^5	1.3×10^8	0.25	101
αCD33xMIC7 with **7**	PROTAC	34	5.6×10^3	1.0×10^5	3.8	140
αEGFRxMIC7 with **6**	PROTAC	66	3.2×10^3	1.3×10^5	3.0	280

PROTAC-complexed αCD33xMIC7 PROxAb Shuttles elicit antitumor responses *in vivo*.

To demonstrate that the PROxAb Shuttle technology not only leads to a drastic half-life prolongation but also enables an efficient delivery of PROTACs into tumors, mouse xenograft studies have been performed. Since the αCD33xMIC7 PROxAb Shuttle complexed with GNE987 demonstrated the highest PROTAC half-life prolongation in the previous PK studies, this combination was further investigated regarding its potential to slow down tumor growth in a tumor-bearing mouse model. The αCD33xMIC7 PROxAb Shuttle was complexed with GNE987 (**6**), the most potent PROTAC in our *in vitro* assays (Tables S1 and S2), at a PROTAC-to-antibody ratio of 2 and the myelomonocytic leukemia cell line MV4-11 was selected as a suitable *in vivo* model. MV4-11 has a moderate CD33 receptor density and was shown to be sensitive towards both, free GNE987 (**6**) and the respective complexed PROxAb Shuttles in previous *in vitro* experiments (Figure 5D). The administered doses of complexed PROxAb Shuttle were matched to equivalent amounts of PROTAC in order to enable a direct comparison between the mice treated with complexed PROxAb Shuttle and PROTAC alone. Figure 7A depicts the tumor growth inhibition curves in female CB17 SCID mice treated either with GNE987 alone (**6**) or complexed and non-complexed αCD33xMIC7 Shuttle, or complexed αCD33xMIC5 Shuttle and a vehicle control. All tested molecules were administered intravenously on day 1 as a single dose. The complexed αCD33xMIC7 PROxAb Shuttle demonstrated superior antitumor activity as compared to an equivalent dose of GNE987 (**6**) alone or the vehicle control (Figure 7C). In addition, the respective non-complexed αCD33xMIC7 Shuttle did not elicit any antitumor effect at all. These results are in line with the prolonged half-life of the PROTAC when complexed with a PROxAb Shuttle, as observed during previous PK studies, and indicate that targeted tumor drug delivery of a PROTAC via the non-covalent PROxAb Shuttle approach results in similar effects as observed for conventional ADCs.[29] Also, the αCD33xMIC5 Shuttle complexed with GNE987 (**6**) was not able to induce a significant antitumor response when compared with the vehicle control, which can likely be attributed to the 21-fold faster off-rate of the MIC5 antibody domain (Table S4). In addition to the accelerated complexation and generation of PROxAb Shuttles, another advantage of the non-covalent versus the covalent interaction could be the application of therapeutic pre-targeting concepts wherein the targeting antibody and the PROTAC are administered separately to enable binding of the antibody to the cells of interest in a first step. Especially for toxic small molecules, pre-targeting has the advantage of minimizing systemic exposure and, therefore, potentially unwanted side effects associated with such non-targeted molecules.[30,31] Recently, Bordeau and coworkers described an approach for a non-covalent and therapeutically focused antibody/small molecule interaction which is based on the concept of re-binding *in vivo*.[32] Their work focused on an antibody that was able to bind to the cytotoxic payload monomethyl auristatin E (MMAE), a toxin that is frequently used in ADC design. The approach aimed at the detoxification of free MMAE originating from the degradation of an MMAE-based ADC *in vivo*, and depends on the co-administration of their anti-MMAE antibody with the ADC. Bordeau and coworkers could demonstrate that the anti-MMAE antibody and free, deconjugated MMAE could bind to one another *in vivo* and, consequently, could diminish common MMAE-related side effects. Intrigued by this concept, we next wanted to elucidate the possibility of re-binding for the PROxAb Shuttle technology. Prior to conducting efficacy experiments in tumor-bearing mice, we first investigated the re-binding ability of a PROxAb Shuttle by performing PK studies in which we sequentially administered a non-complexed αCD33xMIC7 PROxAb Shuttle followed by administration of the PROTAC GNE987P (**7**) 24 hours later (Figure S5). The resulting plasma profiles of pre-complexed αCD33xMIC7 were nearly identical to the plasma profile after sequential administration of the αCD33xMIC7 Shuttle and GNE987P (**7**) (with half-lives of 33.6 and 25.2 hours, respectively), demonstrating the possibility of *in vivo* complexation between our PROxAb Shuttle and free PROTAC. Motivated by these results, we treated MV4-11 tumor-bearing mice with the αCD33xMIC7 PROxAb Shuttle complexed with GNE987 (**6**) on day 1 (PROTAC-to-antibody ratio of 2) and re-dosed mice with GNE987 (**6**) alone on day 8. This interval was chosen based on previous total antibody plasma profiles of αCD33xMIC7. Of note, the dose of GNE987 (**6**) administered on day 8 was equivalent to the dose received on day 1. As can be seen in Figure 7C and E, re-dosing of the PROTAC to the Shuttle could prolong the efficacy of the αCD33xMIC7 PROxAb Shuttle by several days as compared to the group that did not undergo the re-dosing treatment. Moreover, the antitumor effect of the PROxAb Shuttle was significantly more pronounced when compared to the group that solely received doses of free PROTAC on day 1 and day 8. Importantly, the PROxAb Shuttles were well-tolerated, and no body weight loss was observed (Figure S6). Dedicated experiments that focus on sequential administration of a non-complexed Shuttle and PROTAC alone are currently under investigation by our group. Such studies could open avenues for the direct assembly of non-covalent ADCs *in vivo* and for utilizing sequential loading of one PROxAb Shuttle with PROTACs targeting different proteins to maximize patient benefit in a highly personalized approach.

The camelid-derived MIC7 VHH antibody domain can be humanized to yield therapeutic PROxAb Shuttle candidates.

The reduction of potential immunogenicity and the associated side effects, such as rapid clearance or neutralization of the antibody drug, remain an essential pillar in antibody drug development. To address this, we sought to humanize the camelid-derived antibody domain MIC7 which we employed in our best-performing PROxAb Shuttles. Humanization of camelid antibody domains was first described by Vincke and coworkers in 2009 and was since developed into an established protocol that is widely applied to therapeutic nanobodies, culminating in the approval of the humanized nanobody caplacizumab.[33,34] Leveraging our recently described approach for *in silico* sequence assessment, the humanization strategy that was employed for MIC7 started with a sequence-alignment with the most similar human germline sequence and, subsequently, relied on the modification of

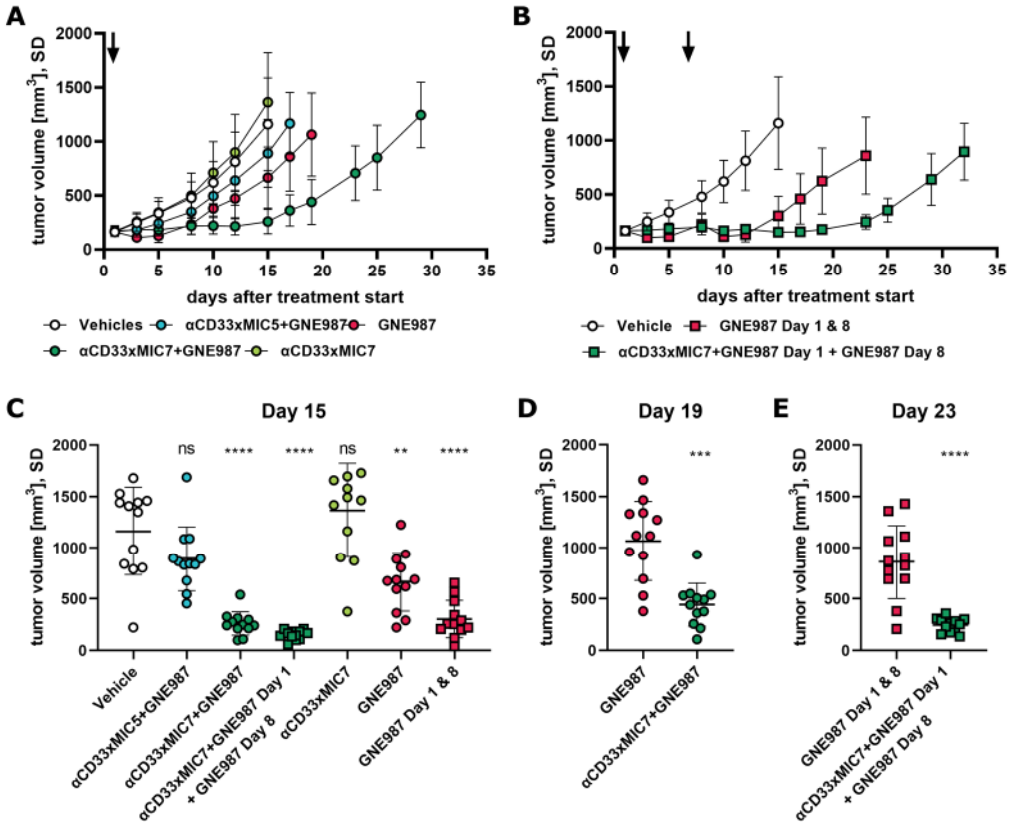

Figure 7. Results of *in vivo* efficacy studies in tumor-bearing mice. A) The αCD33xMIC5 and αCD33xMIC7 PROxAb Shuttles in a complexed and non-complexed form were administered to MV4-11 tumor-bearing mice at a dose of 30 mg/kg. The PROTAC-to-antibody ratio was set to 2 for each Shuttle. Free GNE987 PROTAC (**6**) was administered at a dose equivalent to complexed GNE987 (**6**) in the PROxAb Shuttles (i.e. 0.38 mg/kg). The arrow indicates the time of drug administration. B) Free GNE987 (**6**) as well as GNE987-complexed αCD33xMIC7 PROxAb Shuttle were administered to MV4-11 tumor-bearing mice at doses of 0.38 mg/kg and 30 mg/kg, respectively. Re-dosing of GNE987 (**6**) at 0.38 mg/kg was performed in both groups on day 8. Arrows indicate the time of drug administration. C), D) and E) End point analyses of the *in vivo* efficacy study depicted in A) on days 15, 19 and 23, respectively. Significance levels were determined by Two-Way ANOVA (C) and two-tailed, unpaired t-Test (D and E).

residues which were located outside of critical structural positions (Vernier and Hallmark positions) in order to preserve the structural integrity of the CDRs.[35] Building on these initial mutations, additional humanized MIC7 variants were generated by adding the humanized residues in these key structural positions in a step-by-step process. The resulting humanized MIC7 mutant domains (hMIC7_1.X) were fused to the αCD33 antibody to generate full-length PROxAb Shuttles. The affinity towards VH032 (**5**) was confirmed *via* ITC (Table S5) and SPR (Table S6).

Table 3. Potencies of humanized and wildtype αCD33 PROxAb Shuttles complexed with GNE987 (**6**) or GNE987P (**7**) at a PROTAC-to-antibody ratio of 1 on CD33-positive MV4-11 and MOLM13 as well as CD33-negative RAMOS cells. Potencies of PROTAC GNE987 (**6**) and GNE987P (**6**) alone have also been included for comparison.

		IC_{50} [M]		
Shuttle	**PROTAC**	**MV4-11**	**MOLM13**	**RAMOS**
αCD33xhMIC7_1.6	**6**	<3.0 x 10^{-11}	6.6 x 10^{-11}	> 1.0 x 10^{-7}
αCD33xMIC7	**6**	3.6 x 10^{-11}	1.3 x 10^{-9}	> 1.0 x 10^{-7}
-	**6**	6.7 x 10^{-12}	2.3 x 10^{-11}	1.3 x 10^{-10}
αCD33xhMIC7_1.6	**7**	7.9 x 10^{-11}	9.2 x 10^{-10}	> 1.0 x 10^{-7}
αCD33xMIC7	**7**	8.4 x 10^{-11}	2.1 x 10^{-9}	> 1.0 x 10^{-7}
-	**7**	2.9 x 10^{-10}	1.6 x 10^{-9}	1.7 x 10^{-8}

Using ITC, we could also confirm the stoichiometries of N = 2 or 2.1 for all humanized MIC7 variants. The fully humanized αCD33xhMIC7_1.6 Shuttle variant comprising the most mutations was able to elicit selective cell killing in the same potency range as αCD33 PROxAb Shuttles with non-humanized MIC7 domains (Table 3). Taken together, hMIC7_1.6-based PROxAb Shuttles performed similar when compared to their non-humanized MIC7 precursor in terms of protein production, stability, binding affinity as well as *in vitro* cytotoxicity.

Conclusion

Rising interest in the field of Targeted Protein Degradation has culminated in the transition of the first PROTACs into advanced clinical trials.[1] Despite their catalytic mode of action and ability to engage therapeutic targets which are often intractable for conventional inhibitors, developing cell type-specific PROTACs remains a challenge. Covalent antibody-PROTAC conjugates have recently been reported, combining the cellular specificity of an antibody with the cell killing properties of a PROTAC.[4,5,8,12] Nevertheless, the heterobifunctional nature of PROTACs often impedes the identification of suitable and generic attachment sites for chemical linkers, resulting in time- and resource-consuming efforts. Herein, we describe the identification and therapeutic application of camelid-derived single domain antibodies which bind to the E3 ligase-recruiting subunit of a PROTAC with single-digit nano- to subnanomolar affinities. Specifically, antibodies that engage VH032-based PROTACs which recruit the VHL E3 ubiquitin ligase, one of the most frequently leveraged ligases for PROTAC design, have been identified in the scope of this work. Fusing the camelid antibody domain to therapeutic human antibody scaffolds resulted in bispecific, multivalent fusion proteins that build strong non-covalent complexes with PROTACs at defined PROTAC-to-antibody ratios. These complexes effectively deliver PROTACs to target cells and selectively induce cell killing. Notably, the *in vivo* half-life of PROTACs bound by PROxAb Shuttles was prolonged from a few hours to several days and the complexes induced antitumor responses in

mouse xenograft models comparable to effects observed for conventional ADCs. In addition, we demonstrated that re-dosing of the PROTAC alone to tumor-bearing mice which were pre-dosed with complexed PROxAb Shuttle can further prolong tumor growth control by the Shuttle. Fine-tuning of PK- and efficacy parameters by affinity maturation of the antibody/PROTAC interaction is expected to enable the design of PROxAb Shuttles with tailor-made characteristics. The therapeutic potential of this approach is further underlined by the straightforward humanization strategies that have been implemented for camelid-derived VHH domains over the past years and that have culminated in the FDA-approval of the humanized VHH variant caplazicumab.[23,33,34]

Our non-covalent PROxAb Shuttle complexes can be generated rapidly and in a matter of only a few minutes at the bench whereas the covalent conjugation of PROTACs to antibodies has proven to be challenging and time-consuming in the past. The PROxAb Shuttle technology could enable scientists to assess degrader candidates which have not been optimized with regards to PK profile or cellular permeability, both *in vitro* and *in vivo*. In summary, the PROxAb Shuttle technology represents a plug-and-play platform for the rapid generation of VH032-based antibody-PROTAC complexes and has the potential to rescue PROTACs which may not be suitable for clinical development as a monotherapy due to limitations regarding *in vivo* toxicity or reaching sufficient oral bioavailability.

Acknowledgements

The authors would like to sincerely thank the following people at Merck KGaA, Darmstadt, Germany who have contributed to the experiments and results presented in the scope of this publication: Andreas Schönemann for SPR measurements, Frank Fischer, Djordje Musil, Martin Lehmann, Ralf Günther, Thomas Eichhorn, Sabine Raab-Westphal, Kevin Heitland, Stephanie Czasch, Ilse de Salve, Elisa Bertotti, Patrizia Tavano, Jens Hannewald, Ingrid Schmidt, Laura Basset, Eva Maria Leibrock, Yvonne Bischoff, Vanessa Lautenbach and Anja Ogroske. In addition, the authors would like to thank Paul Gehrtz for the synthesis of the VH032-pHAb dye and the following companies for their services: preclinics GmbH, YUMAB GmbH and Reaction Biology Corp..

Conflict of Interest

HS, MR, SJ, DK, NR, CS and AE are employees of Merck KGaA, Darmstadt, Germany and inventors on a patent application covering the PROxAb Shuttle technology (WO2023275394A1). PROxAb Shuttle™ is a registered trademark.

Keywords: PROTAC • antibody • antibody drug conjugate • targeted protein degradation • protein engineering •

References

[1] D. Chirnomas, K. R. Hornberger, C. M. Crews, *Nat. Rev. Clin. Oncol.* **2023**, DOI 10.1038/s41571-023-00736-3.
[2] H. Zhu, J. Wang, Q. Zhang, X. Pan, J. Zhang, *Pharmacol. Ther.* **2023**, *244*, 108371.
[3] L. T. Kramer, X. Zhang, *Curr. Res. Chem. Biol.* **2022**, *2*, 100020.
[4] M. Maneiro, N. Forte, M. M. Shchepinova, C. S. Kounde, V. Chudasama, J. R. Baker, E. W. Tate, *ACS Chem. Biol.* **2020**, *15*, 1306–1312.
[5] T. H. Pillow, P. Adhikari, R. A. Blake, J. Chen, G. Del Rosario, G. Deshmukh, I. Figueroa, K. E. Gascoigne, A. V. Kamath, S. Kaufman, T. Kleinheinz, K. R. Kozak, B. Latifi, D. D. Leipold, C. Sing Li, R. Li, M. M. Mulvihill, A. O'Donohue, R. K. Rowntree, J. D. Sadowsky, J. Wai, X. Wang, C. Wu, Z. Xu, H. Yao, S. Yu, D. Zhang, R. Zang, H. Zhang, H. Zhou, X. Zhu, P. S. Dragovich, *ChemMedChem* **2020**, *15*, 17–25.
[6] G. M. Burslem, J. Song, X. Chen, J. Hines, C. M. Crews, *J. Am. Chem. Soc.* **2018**, *140*, 16428–16432.
[7] V. G. Klein, C. E. Townsend, A. Testa, M. Zengerle, C. Maniaci, S. J. Hughes, K.-H. Chan, A. Ciulli, R. S. Lokey, *ACS Med. Chem. Lett.* **2020**, *11*, 1732–1738.
[8] P. S. Dragovich, T. H. Pillow, R. A. Blake, J. D. Sadowsky, E. Adaligil, P. Adhikari, S. Bhakta, N. Blaquiere, J. Chen, J. dela Cruz-Chuh, K. E. Gascoigne, S. J. Hartman, M. He, S. Kaufman, T. Kleinheinz, K. R. Kozak, L. Liu, L. Liu, Q. Liu, Y. Lu, F. Meng, M. M. Mulvihill, A. O'Donohue, R. K. Rowntree, L. R. Staben, S. T. Staben, J. Wai, J. Wang, B. Wei, C. Wilson, J. Xin, Z. Xu, H. Yao, D. Zhang, H. Zhang, H. Zhou, X. Zhu, *J. Med. Chem.* **2021**, *64*, 2534–2575.
[9] C. Kofink, N. Trainor, B. Mair, S. Wöhrle, M. Wurm, N. Mischerikow, M. J. Roy, G. Bader, P. Greb, G. Garavel, E. Diers, R. McLennan, C. Whitworth, V. Vetma, K. Rumpel, M. Scharnweber, J. E. Fuchs, T. Gerstberger, Y. Cui, G. Gremel, P. Chetta, S. Hopf, N. Budano, J. Rinnenthal, G. Gmaschitz, M. Mayer, M. Koegl, A. Ciulli, H. Weinstabl, W. Farnaby, *Nat. Commun.* **2022**, *13*, 5969.
[10] K. B. Hong, H. An, *J. Med. Chem.* **2023**, *66*, 140–148.
[11] C. Dumontet, J. M. Reichert, P. D. Senter, J. M. Lambert, A. Beck, *Nat. Rev. Drug Discov.* **2023**, *22*, 641–661.
[12] P. S. Dragovich, T. H. Pillow, R. A. Blake, J. D. Sadowsky, E. Adaligil, P. Adhikari, J. Chen, N. Corr, J. dela Cruz-Chuh, G. Del Rosario, A. Fullerton, S. J. Hartman, F. Jiang, S. Kaufman, T. Kleinheinz, K. R. Kozak, L. Liu, Y. Lu, M. M. Mulvihill, J. M. Murray, A. O'Donohue, R. K. Rowntree, W. S. Sawyer, L. R. Staben, J. Wai, J. Wang, B. Wei, W. Wei, Z. Xu, H. Yao, S.-F. Yu, D. Zhang, H. Zhang, S. Zhang, Y. Zhao, H. Zhou, X. Zhu, *J. Med. Chem.* **2021**, *64*, 2576–2607.
[13] H. Marei, W.-T. K. Tsai, Y.-S. Kee, K. Ruiz, J. He, C. Cox, T. Sun, S. Penikalapati, P. Dwivedi, M. Choi, D. Kan, P. Saenz-Lopez, K. Dorighi, P. Zhang, Y. T. Kschonsak, N. Kljavin, D. Amin, I. Kim, A. G. Mancini, T. Nguyen, C. Wang, E. Janezic, A. Doan, E. Mai, H. Xi, C. Gu, M. Heinlein, B. Biehs, J. Wu, I. Lehoux, S. Harris, L. Comps-Agrar, D. Seshasayee, F. J. de Sauvage, M. Grimmer, J. Li, N. J. Agard, F. de Sousa e Melo, *Nature* **2022**, *610*, 182–189.
[14] J. Liu, H. Chen, Y. Liu, Y. Shen, F. Meng, H. Ü. Kaniskan, J. Jin, W. Wei, *J. Am. Chem. Soc.* **2021**, *143*, 7380–7387.
[15] S. He, F. Gao, J. Ma, H. Ma, G. Dong, C. Sheng, *Angew. Chemie Int. Ed.* **2021**, *60*, 23299–23305.
[16] J. Gao, B. Hou, Q. Zhu, L. Yang, X. Jiang, Z. Zou, X. Li, T. Xu, M. Zheng, Y.-H. Chen, Z. Xu, H. Xu, H. Yu, *Nat. Commun.* **2022**, *13*, 4318.
[17] N. Gupta, A. Ansari, G. V. Dhoke, M. Chilamari, J. Sivaccumar, S. Kumari, S. Chatterjee, R. Goyal, P. K. Dutta, M. Samarla, M. Mukherjee, A. Sarkar, S. K. Mandal, V. Rai, G. Biswas, A. Sengupta, S. Roy, M. Roy, S. Sengupta, *Nat. Biomed. Eng.* **2019**, *3*, 917–929.
[18] S. Metz, A. K. Haas, K. Daub, R. Croasdale, J. Stracke, W. Lau, G. Georges, H.-P. Josel, S. Dziadek, K.-P. Hopfner, A. Lammens, W. Scheuer, E. Hoffmann, O. Mundigl, U. Brinkmann, *Proc. Natl. Acad. Sci.* **2011**, *108*, 8194–8199.
[19] B. Schneider, M. Grote, M. John, A. Haas, B. Bramlage, L. M. Lckenstein, K. Jahn-Hofmann, F. Bauss, W. Cheng, R. Croasdale, K. Daub, S. Dill, E. Hoffmann, W. Lau, H. Burtscher, J. L. Ludtke, S. Metz, O. Mundigl, Z. C. Neal, W. Scheuer, J. Stracke, H. Herweijer, U. Brinkmann, *Mol. Ther. Nucleic Acids* **2012**, *1*, e46.
[20] J. Jin, G. Park, J. B. Park, S. Kim, H. Kim, J. Chung, *Exp. Mol. Med.* **2018**, *50*, 1–14.
[21] D. Könning, S. Zielonka, J. Grzeschik, M. Empting, B. Valldorf, S. Krah, C. Schröter, C. Sellmann, B. Hock, H. Kolmar, *Curr. Opin. Struct. Biol.* **2017**, *45*, 10–16.
[22] G. Gonzalez-Sapienza, M. A. Rossotti, S. Tabares-da Rosa, *Front. Immunol.* **2017**, *8*, DOI 10.3389/fimmu.2017.00977.
[23] A. L. Hollifield, J. R. Arnall, D. C. Moore, *Am. J. Heal. Pharm.* **2020**, *77*, 1201–1207.
[24] D. Yanakieva, L. Pekar, A. Evers, M. Fleischer, S. Keller, D. Mueller-Pompalla, L. Toleikis, H. Kolmar, S. Zielonka, S. Krah, *MAbs* **2022**, *14*, DOI 10.1080/19420862.2021.2018960.
[25] A. C. Phillips, E. R. Boghaert, K. S. Vaidya, M. J. Mitten, S. Norvell, H. D. Falls, P. J. DeVries, D. Cheng, J. A. Meulbroek, F. G. Buchanan, L. M. McKay, N. C. Goodwin, E. B. Reilly, *Mol. Cancer Ther.* **2016**, *15*, 661–9.
[26] M. S. Kung Sutherland, R. B. Walter, S. C. Jeffrey, P. J. Burke, C. Yu, H. Kostner, I. Stone, M. C. Ryan, D. Sussman, R. P. Lyon, W. Zeng, K. H. Harrington, K. Klussman, L. Westendorf, D. Meyer, I. D. Bernstein, P. D. Senter, D. R. Benjamin, J. G. Drachman, J. A. McEarchern, *Blood* **2013**, *122*, 1455–1463.
[27] Y.-C. Han, J. Kahler, N. Piché-Nicholas, W. Hu, S. Thibault, F. Jiang, M. Leal, M. Katragadda, A. Maderna, R. Dushin, N. Prashad, M. B. Charati, T. Clark, L. N. Tumey, X. Tan, A. Giannakou, E. Rosfjord, H.-P. Gerber, L. Tchistiakova, F. Loganzo, C. J. O'Donnell, P. Sapra, *Clin. Cancer Res.* **2021**, *27*, 622–631.
[28] S. Dengl, C. Sustmann, U. Brinkmann, *Immunol. Rev.* **2016**, *270*, 165–177.
[29] A. J. Ocean, A. N. Starodub, A. Bardia, L. T. Vahdat, S. J. Isakoff, M. Guarino, W. A. Messersmith, V. J. Picozzi, I. A. Mayer, W. A. Wegener, P. Maliakal, S. V. Govindan, R. M. Sharkey, D. M. Goldenberg, *Cancer* **2017**, *123*, 3843–3854.
[30] F. C. J. van de Watering, M. Rijpkema, L. Perk, U. Brinkmann, W. J. G. Oyen, O. C. Boerman, *Biomed Res. Int.* **2014**, *2014*, 1–13.

[31] F. Kraeber-Bodéré, C. Rousseau, C. Bodet-Milin, E. Frampas, A. Faivre-Chauvet, A. Rauscher, R. M. Sharkey, D. M. Goldenberg, J.-F. Chatal, J. Barbet, *Front. Pharmacol.* **2015**, *6*, DOI 10.3389/fphar.2015.00054.
[32] B. M. Bordeau, T. D. Nguyen, J. R. Polli, P. Chen, J. P. Balthasar, *Mol. Cancer Ther.* **2023**, *22*, 459–470.
[33] C. Vincke, R. Loris, D. Saerens, S. Martinez-Rodriguez, S. Muyldermans, K. Conrath, *J. Biol. Chem.* **2009**, *284*, 3273–3284.
[34] H. T. Lee, U. B. Park, T. J. Jeong, N. Gu, S. H. Lee, Y. Kim, Y.-S. Heo, *Biochem. Biophys. Res. Commun.* **2021**, *567*, 49–55.
[35] A. Evers, S. Malhotra, W.-G. Bolick, A. Najafian, M. Borisovska, S. Warszawski, Y. Fomekong Nanfack, D. Kuhn, F. Rippmann, A. Crespo, V. Sood, **2023**, pp. 383–398.

PROxAb Shuttle: A non-covalent plug-and-play platform for the rapid generation of tumor-targeting antibody-PROTAC conjugates

Hendrik Schneider[a], Sebastian Jäger[a], Doreen Könning[a], Nicolas Rasche[a], Christian Schröter[a], Desislava Elter[a], Andreas Evers[a], Marc Lecomte[a], Federico Riccardi Sirtori[b], Daniel Schwarz[a], Ansgar Wegener[a], Ingo Hartung[a] and Marcel Rieker*[a]

[a]Merck KGaA, Darmstadt, Germany; Frankfurter Strasse 250, 64293 Darmstadt, Germany
[b]Merck KGaA, RBM S.p.A., Via Ribes 1, 10010 Colleretto Giacosa (TO), Italy

*Corresponding Author: marcel.rieker@merckgroup.com

Supporting Information

Table of Contents

Experimental Procedures

Materials

All chemicals, building blocks and reagents were purchased from commercial sources such as Sigma-Aldrich Corp., abcr GmbH, Thermo Fisher Scientific Inc., Merck KGaA, Bio-Techne GmbH, and VWR International, Medchemexpress®, and used without any further purification unless otherwise stated. (S,R,S)-AHPC-PEG_3-NH_2 hydrochloride, and (S,R,S)-AHPC-C_6-CO_2H hydrochloride **4** (VHL-c) were acquired from Sigma Aldrich. GNE987 (**6**), GNE987P (**7**, PROTAC BRD4 Degrader-8), ARV771 (**8**), SIM1 (**13**), SIAIS178 and (**14**) were acquired from MedChemExpress®, USA. AT1 (**12**) was acquired from Tocris Biosience, UK. All PROTACs and building blocks were used without any further purification unless otherwise stated.

Synthesis of Hapten 1 (VHL-1)

2-(2-(2-(((S)-1-((2S,4R)-4-hydroxy-2-((4-(4-methylthiazol-5-yl)benzyl)carbamoyl)pyrrolidin-1-yl)-3,3-dimethyl-1-oxobutan-2-yl)amino)-2-oxoethoxy)ethoxy)acetic acid (CAS: 2172820-08-3)

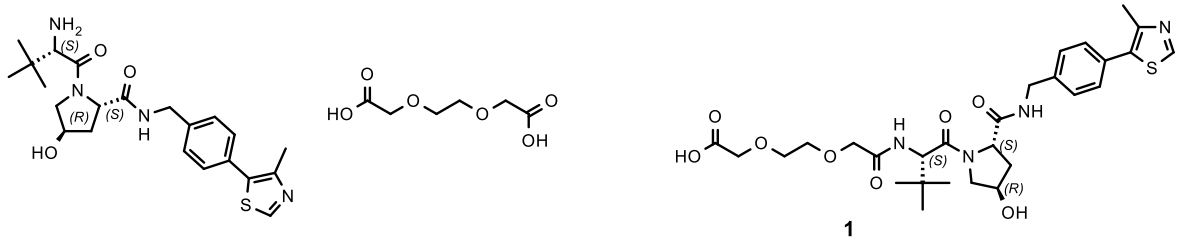

1

This compound was synthesized according to literature procedure.[1]
HPLC-MS: RT = 1.26 min, m/z $(M+H)^+$ = 591
Method Info : A: H_2O + 0.05% HCOOH | B: MeCN + 0.04% HCOOH
T: 45°C | Flow: 3.3 mL/min | MS: 61-1000 amu positive
Column: Chromolith HR RP-18e 50-4.6 mm
1% -> 99% B: 0 -> 2.0 min | 99% B: 2.0 -> 2.5 min

Synthesis of Hapten 2 (VHL-6)

(S)-16-((2S,4R)-4-hydroxy-2-((4-(4-methylthiazol-5-yl)benzyl)carbamoyl)pyrrolidine-1-carbonyl)-17,17-dimethyl-14-oxo-3,6,9,12-tetraoxa-15-azaoctadecanoic acid (CAS: 2360516-50-1)

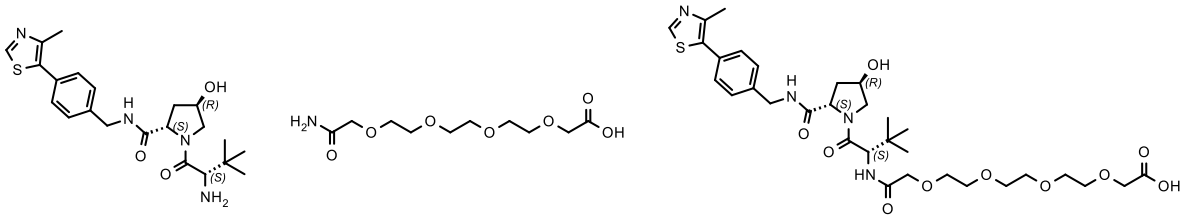

2

This compound was synthesized according to literature procedure (*MERCK KGAA - WO2023/78813, 2023, A1; Location in patent: Page/Page column 155*).
HPLC-MS: RT = 1.3 min, m/z $(M+H)^+$ = 679
Method Info : A: H_2O + 0.05% HCOOH | B: MeCN + 0.04% HCOOH
T: 40°C | Flow: 3.3 mL/min | MS: 100-2000 amu positive
Column: Chromolith HR RP-18e 50-4.6 mm
0% -> 100% B: 0 -> 2.0 min | 100% B: 2.0 -> 2.5 min

Synthesis of Hapten 3 (VHL-7)

(S)-19-((2S,4R)-4-hydroxy-2-((4-(4-methylthiazol-5-yl)benzyl)carbamoyl)pyrrolidine-1-carbonyl)-20,20-dimethyl-17-oxo-3,6,9,12,15-pentaoxa-18-azahenicosanoic acid (CAS: 2172820-13-0)

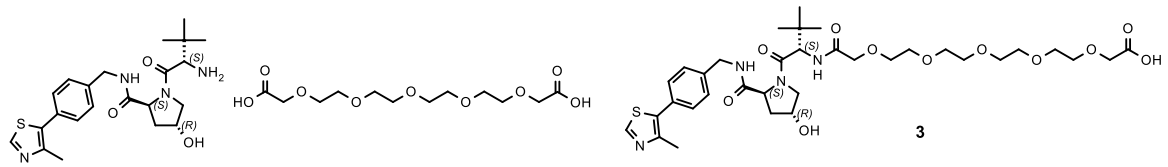

3

This compound was synthesized according to literature procedure.[2]
HPLC-MS: RT = 1.33 min, m/z $(M+H)^+$ = 723
Method Info : A: H_2O + 0.05% HCOOH | B: MeCN + 0.04% HCOOH
T: 40°C | Flow: 3.3 mL/min | MS: 100-2000 amu positive
Column: Chromolith HR RP-18e 50-4.6 mm
0% -> 100% B: 0 -> 2.0 min | 100% B: 2.0 -> 2.5 min

Synthesis of 11 (cMETd1)

N1'-(3-fluoro-4-((7-(3-(3-(3-(((S)-1-((2S,4S)-4-hydroxy-2-((4-(4-methylthiazol-5-yl)benzyl)carbamoyl)pyrrolidin-1-yl)-3,3-dimethyl-1-oxobutan-2-yl)amino)-3-oxopropoxy)propoxy)propoxy)-6-methoxyquinolin-4-yl)oxy)phenyl)-N1-(4-fluorophenyl)cyclopropane-1,1-dicarboxamide (CAS: 2230821-69-7)

Compound **11** was synthesized according to literature procedure (*ARVINAS - WO2018/226542, 2018, A1, Location in patent: Paragraph 00373*) starting from N-[3-Fluoro-4-[(7-hydroxy-6-methoxy-4-quinolinyl)oxy]phenyl]-N′-(4-fluorophenyl)-1,1-cyclopropanedicarboxamide (CAS: 849217-50-1)
UPLC-MS: HPLC-MS: RT = 0.701 min, m/z $(M+2H)^{2+}$ = 554
System: Waters Acquity UPLC
Method: A: H_2O + 0,05% HCOOH | B: MeCN + 0.04% HCOOH + 1% H_2O
T: 40°C | Flow: 0.9 mL/min | Column: Kinetex EVO-C18 1.7 µm 50-2.1 mm
1% -> 99% B: 0 -> 1.0 min | 99% B: 1.0 -> 1.3 min

Synthesis of pH responsive dye 15 (VH032-pHAb dye)

1-(9-{2-carboxylato-5-[(2-{2-[2-({[(2S)-1-[(2S,4R)-4-hydroxy-2-({[4-(4-methyl-1,3-thiazol-5-yl)phenyl]methyl}carbamoyl)pyrrolidin-1-yl]-3,3-dimethyl-1-oxobutan-2-yl]carbamoyl}methoxy)ethoxy]ethoxy}ethyl)carbamoyl]phenyl}-6-[4-(4-sulfobutyl)piperazin-1-yl]-3H-xanthen-3-ylidene)-4-(4-sulfobutyl)-1lambda5-piperazin-1-ylium

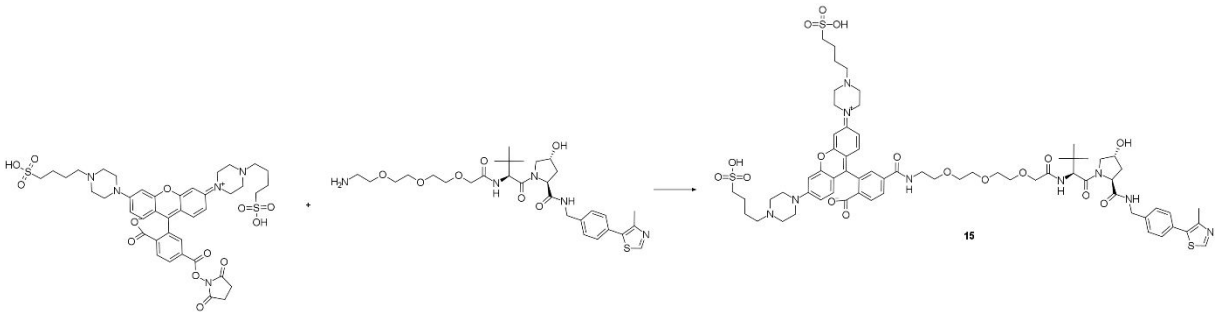

A 0.5 mL septum-sealed microwave vial with stir flea was heated with a heat gun under vacuum and cooled down under a flow of argon gas (needle technique). 1-[9-(2-carboxylato-5-{[(2,5-dioxopyrrolidin-1-yl)oxy]carbonyl}phenyl)-6-[4-(4-sulfobutyl)piperazin-1-yl]-3H-xanthen-3-ylidene]-4-(4-sulfobutyl)-1lambda5-piperazin-1-ylium (3 mg; 3.4 µmol; 1 eq.) (12 x 250 µg dry aliquots) were dissolved in a total of 250 µL dry DMSO. The pink solution was immediately transferred to the reaction vessel, and 1-[9-(2-carboxylato-5-{[(2,5-dioxopyrrolidin-1-yl)oxy]carbonyl}phenyl)-6-[4-(4-sulfobutyl)piperazin-1-yl]-3H-xanthen-3-ylidene]-4-(4-sulfobutyl)-1lambda5-piperazin-1-ylium (3 mg; 3.4 µmol; 1 eq.) was added, followed by *N*-ethyldiisopropylamine ($^{i}Pr_2NEt$) (12 µL; 68 µmol; 20 eq.) as a base. The vessel was sealed and fitted with an argon balloon *via* the septum. The reaction mixture was shielded from light by cardboard boxes and stirred at RT, which led to a deep purple solution. The reaction mixture was stirred overnight at RT, diluted with 750 µL DMSO and purified by preparative RP-HPLC-MS (Sunfire column). Target fractions were lyophilized under light exclusion, giving a pink-purple solid as the product.
HPLC-MS: RT = 1.76 min, m/z $(M+2H)^{2+}$ = 693
Method Info : A: H_2O + 0.05% HCOOH | B: MeCN + 0.04% HCOOH + 1% H_2O
T: 40°C | Flow: 1.4 mL/min | MS: 61-1000 amu positive
Column: SunFire C18 5.0 µm 100-3 mm
1% -> 99% B: 0 -> 2.0 min | 99% B: 2.0 -> 2.7 min

Synthesis of BETTY2 (9, here: compound 1) and BETTY3 (10, here: compound 2) by ChemPartner, China.

Synthesis Scheme

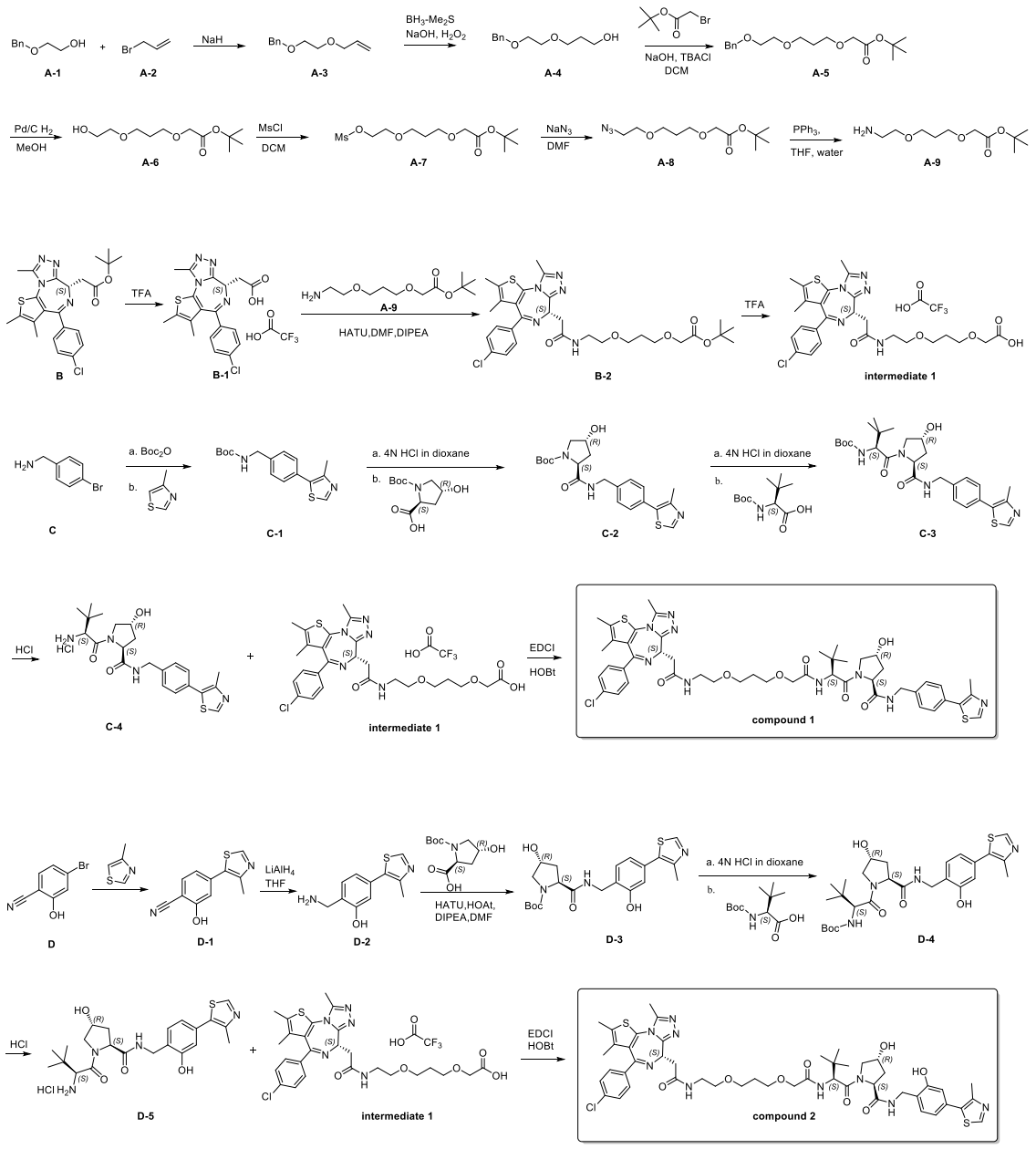

Synthesis of compound A-3

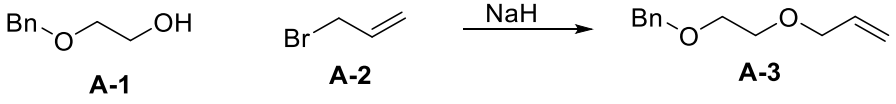

To a solution of compound A-1 (30 g, 197 mmol) in tetrahydrofuran (THF) (400 mL) was carefully added sodium hydride (9.46 g, 237 mmol) and compound A-2 (28.6 g, 237 mmol) at 0 °C. The reaction mixture was stirred at 20 °C for 16 hours, quenched with water (~ 100 mL), partitioned with ethyl acetate (700 mL) and water (200 mL). The organic layer was washed with saturated aqueous sodium chloride (100 mL), dried with anhydrous sodium sulfate, filtered and evaporated to give compound A-3 as yellow oil (35 g, yield: 91%).

Synthesis of compound A-4

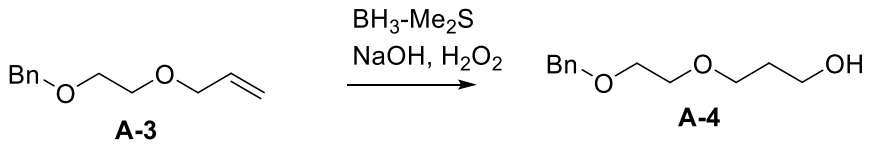

To a mixture of compound A-3 (35 g, 182.3 12.09 mmol) in THF (200 mL) was added borane dimethylsulfide (BH_3-Me_2S) (10 M, 27 mL) dropwise at 0 °C under nitrogen (N_2) and the resulting mixture was stirred at RT for 2 hours. TLC indicated starting material was consumed completely and one major new spot was detected. Then H_2O (124 mL), NaOH (3 M, 14 mL) and H_2O_2 (146 g, 1292.5 mmol, 124 mL, 30% wt) were added sequentially to this reaction at 0 °C and the resulting mixture was allowed to stir another 2 hours at 20 °C. TLC indicated starting material was consumed completely. The reaction mixture was quenched with saturated Na_2CO_3 (150 mL) and extracted with EtOAc (150 mL x 3). The organic layer was dried over Na_2SO_4, filtered and concentrated. The residue was purified by column chromatography (SiO_2, Petroleum ether/Ethyl acetate=10/1 to 1/1) to afford compound A-4 as a colorless oil (16 g, yield: 41%).

Synthesis of compound A-5

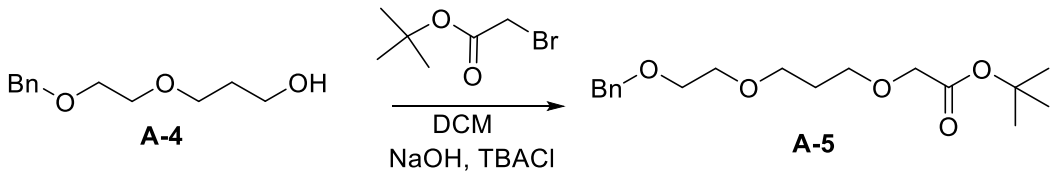

A mixture of compound A-4 (16 g, 76 mmol), tert-butyl bromoacetate (45.0 mL, 304 mmol), tetra-n-butylammonium chloride (21.15 g, 76 mmol) and NaOH (76 mL, 761 mmol) in DCM (200 mL) was stirred vigorously for 18 hours. The mixture was concentrated and partitioned between 1000 mL each of ethyl acetate and water. The organic layer was washed with 200 mL of saturated aqueous sodium chloride, dried over anhydrous sodium sulfate, filtered and concentrated. The residue, combined with above batch, was purified by chromatography (silica, 5-100% ethyl acetate in petroleum ether afforded compound A-5 as light yellow oil (14 g, yield:55%).

Synthesis of compound A-6

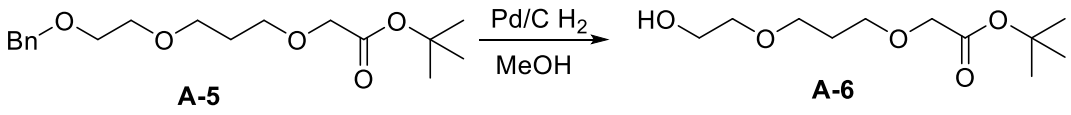

To the mixture of compound A-5 (14 g, 43.2 mmol) in MeOH (150 ml) was added Pd-C (2.76 g, 2.59 mmol) under nitrogen and then the reaction was degassed with hydrogen and stirred under hydrogen for 16 hours. LCMS showed that all the SM had disappeared. The reaction, combined with above batch, was filtered through celite and washed with ethyl acetate. The solvent was removed to give compound A-6 which was used into next step directly (10 g, yield: 94%).

Synthesis of compound A-7

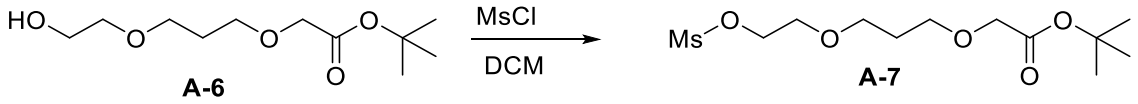

To a solution of compound A-6 (10 g, 42.7 mmol) and TEA (triethylamine) (11.90 mL, 85 mmol) in DCM (300 mL) was added Ms-Cl (methanesulfonyl chloride) (4.99 mL, 64.0 mmol) slowly at 0 °C. Then the reaction mixture was stirred for 3 hr. TLC showed that the starting material had disappeared and a new spot was observed. The reaction mixture was quenched by addition of water (~ 100 mL), then extracted with dichloromethane (100 mL). The combined organic phase was washed with brine (50 mL), dried over sodium sulfate, filtered and concentrated under reduced pressure to afford compound A-7 as colorless liquid, which was used directly for the next step (13 g, yield: 93%).

Synthesis of compound A-8

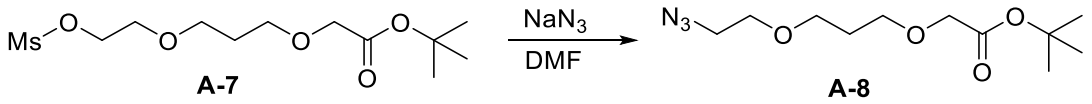

To a solution of compound A-7 (13 g, 41.6 mmol) in DMF (90 ml) was added sodium azide (3.25 g, 49.9 mmol). Then the reaction mixture was stirred at 70 °C for 16 hours. Then water (300 mL) was added and the reaction mixture was extracted with ethyl acetate (200 mL x 2). The combined organic phases were washed with brine (100 mL), dried over sodium sulfate, filtered and concentrated under reduced pressure to give a residue, which was purified by column chromatography eluted with petroleum ether : ethyl acetate = 100:1 to 3:1 to afford compound A-8 as colorless oil (10 g, yield: 93%).

Synthesis of compound A-9

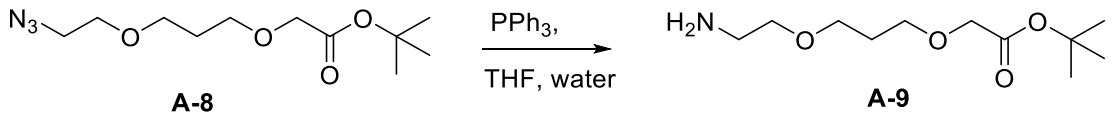

A mixture of compound A-8 (10 g, 36.6 mmol) and triphenylphosphine (14.41 g, 55.0 mmol) in THF (150 ml) / Water (4.55 ml) was stirred at 20 °C for 16 hours. Thin-layer chromatography (TLC) (ninhydrin, 5% methanol in dichloromethane) indicated the reaction was complete. The solvent was removed and the residue was loaded onto silica gel and purified by chromatography (silica, 1-10% methanol/ammonia in dichloromethane) to give compound A-9 as light yellow oil (7.5 g, yield:83%).

Synthesis of compound B-1

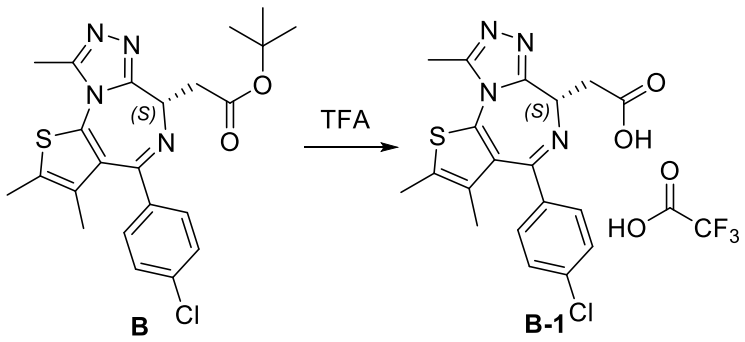

Compound B (5 g, 10.75 mmol) was dissolved in TFA (20 mL). The mixture was stirred at 60 °C for 1 hour. The mixture was concentrated under reduce pressure to afford crude compound B-1 as an yellow solid, which was used in the next step without further purification (6.6 g, TFA salt).

Synthesis of compound B-2

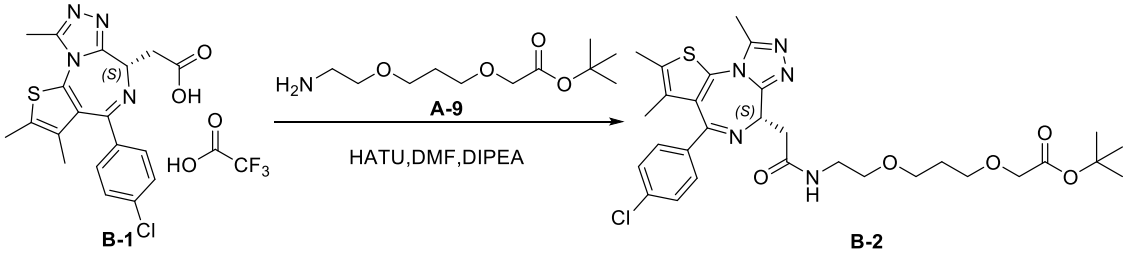

To a solution of compound B-1 (1.2 g, 3.0 mmol), compound A-9 (1.05 g, 4.5 mmol) and HATU (1.7 g, 4.5 mmol) in DMF (15 mL) was added DIPEA (1.56 mL, 9.0 mmol). The mixture was stirred at RT for 1 hour then purified by Reversed-phase chromatography (C18) (0.1% NH_4HCO_3 in water, 0-95%MeCN) to give compound B-2 as a white solid (1.2 g, yield: 67%).

Synthesis of intermediate 1

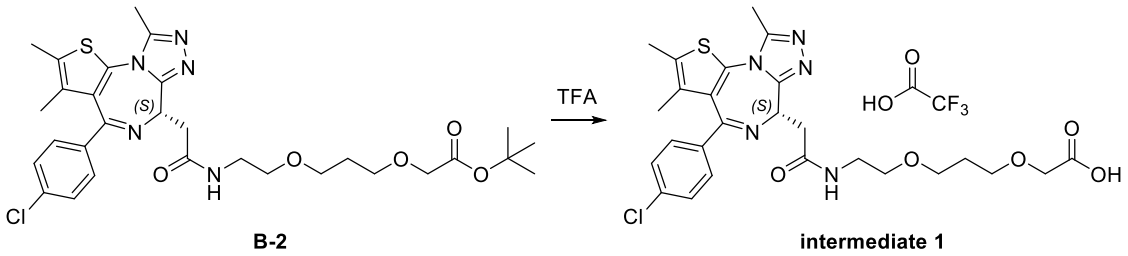

To a solution of compound B-1 (1.2 g, 2.0 mmol) in DCM (10 mL) was added TFA (5 mL) and the mixture was stirred at RT for 2 hours, then the reaction mixture was concentrated under reduced pressure and purified by Reversed-phase chromatography (C18) (0.1% TFA in water, 0-95%MeCN) to give compound intermediate 1 as a yellow solid (950 mg, yield: 73%).

Synthesis of compound C-1

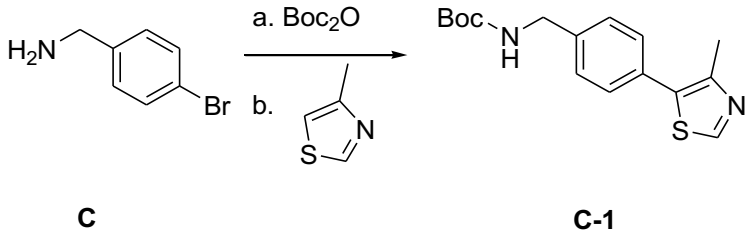

To a mixture of compound C (11.2 g, 60.3 mmol) and $NaHCO_3$ (4.0 g, 48.2 mmol) in water (10 mL) and ethyl acetate (60 mL), $(Boc)_2O$ (15.7 g, 72.4 mmol) at 5 °C was added. The reaction was stirred for 2 hours, TLC showed the reaction was complete. The reaction mixture was filtered. The solid fraction was collected and suspended in a mixture of hexane (40 mL) and water (10 mL) for 0.5 h. The mixture was filtered, and the solid fraction was collected and evaporated to dryness at 50 °C to afford the title compound as a white solid. The solid was dissolved in DMF (40 mL), then 4-methylthiazole (11.9 g, 120.6 mmol), palladium (II) acetate (137 mg, 0.60 mmol), and potassium acetate (11.8 g, 120.6 mmol) was added. The mixture was stirred at 90 °C under nitrogen for 18 h. After cooling to ambient temperature, the reaction mixture was filtered. 50 mL of water was added to the filtrate, and the resulting mixture was stirred at ambient temperature for 4 h. The reaction mixture was filtered. The solid was collected by filtration and dried in an oven at 50 °C to afford compound C-1 as a gray solid (15.3 g, yield: 83%).

Synthesis of compound C-2

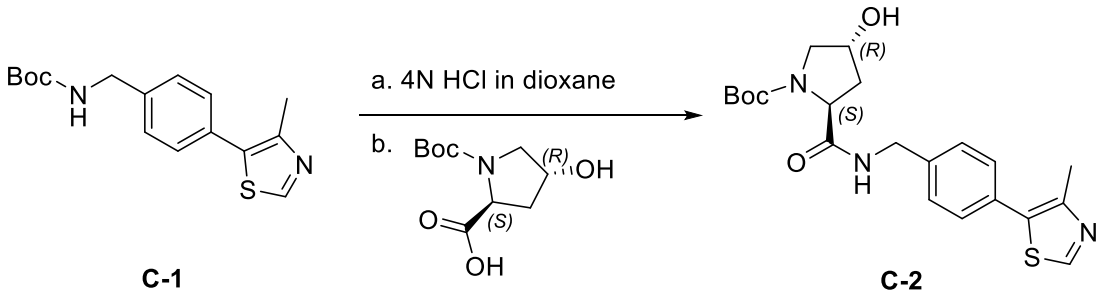

Compound C-1 (15.3 g, 50.3 mmol) was dissolved in 4 N HCl in dioxane (38 mL, 150.9 mmol) and MeOH (35 mL), and the mixture was stirred at ambient temperature for 12 h. The mixture was concentrated, and the residue was dried under vacuum to afford the intermediate. HATU (22.9 g, 60.3 mmol) was added to a solution of this intermediate, (2S,4R)-1-(tert-Butoxycarbonyl)-4-hydroxypyrrolidine-2-carboxylic acid (11.6 g, 50.3 mmol), and DIPEA (26 mL, 150.9 mmol) in DMF (100 mL) at 0 °C under N_2. The mixture was stirred at ambient temperature for 12 hours. TLC showed that the reaction was complete. The reaction mixture was quenched with H_2O (200 mL) and extracted with EtOAc (150 mL x 2). The combined organic layer was washed with brine (200 mL) and dried over Na_2SO_4. The organic solution was filtered and concentrated. The residue was purified by silica gel flash column chromatography with hexane:EtOAc (100:1−1:100), then DCM:MeOH (10:1) to afford the compound C-2 as white solid (18.1 g, yield: 86%).

Synthesis of compound C-2

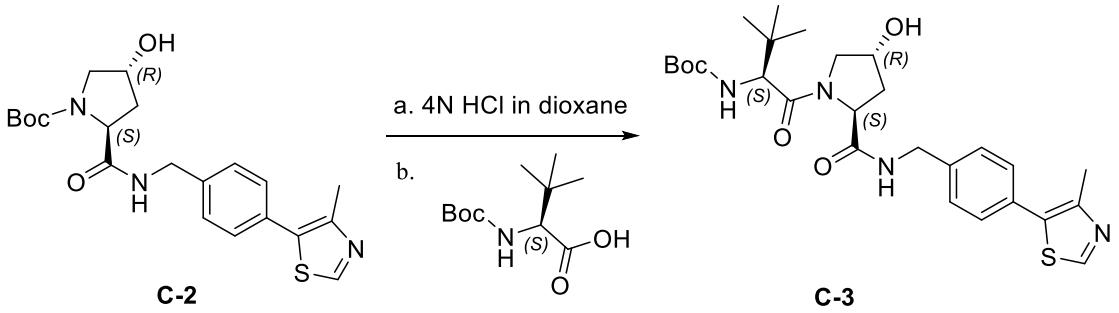

Compound C-2 (16.0 g, 38.3 mmol) was dissolved in 4 N HCl in dioxane (38 mL, 153.2 mmol) and MeOH (38 mL), and the mixture was stirred at ambient temperature for 12 hours. The mixture was then concentrated, and the residue was dried under vacuum to afford intermediate, HATU (21.8 g, 57.4 mmol) was added to a solution of this intermediate, (S)-2-((tert-butoxycarbonyl)amino)-3,3-dimethylbutanoic acid (8.8 g, 38.3 mmol), and DIPEA (20 mL, 114.9 mmol) in DMF (100 mL) at 0 °C under N_2. The mixture was stirred at ambient temperature for 12 hours when TLC showed that the reaction was complete. The reaction mixture was quenched with H_2O (200 mL) and extracted with EtOAc (150 mL x 2). The combined organic layer was washed with brine (100 mL) and dried over Na_2SO_4. The organic solution was filtered and concentrated. The residue was purified by silica gel flash column chromatography with DCM:MeOH (10:1) to afford the desired compound C-3 as an off-white solid (16.0 g, yield: 79%).

Synthesis of compound C-4

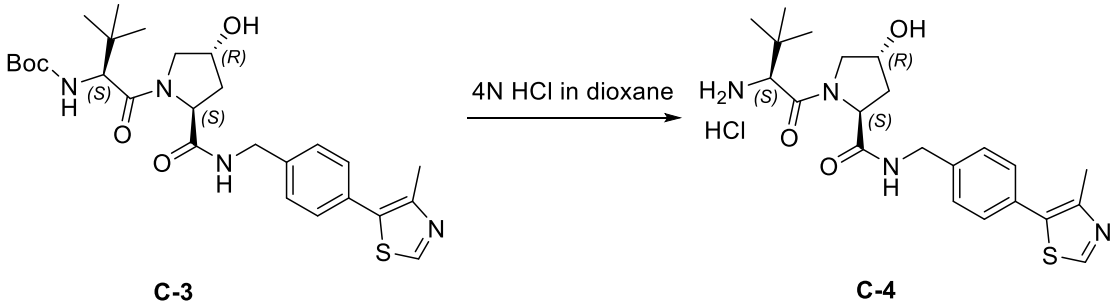

C-3 **C-4**

Compound C-3 (4.0 g, 7.55 mmol) was dissolved in 4 N HCl in dioxane (9.0 mL) and MeOH (9.0 mL), and the mixture was stirred at ambient temperature for 12 h. The mixture was then concentrated, and the residue was dried under vacuum to afford crude compound C-4 as an off-white solid, which was used in the next step without further purification. (4.5 g, HCl salt).

Synthesis of compound 1

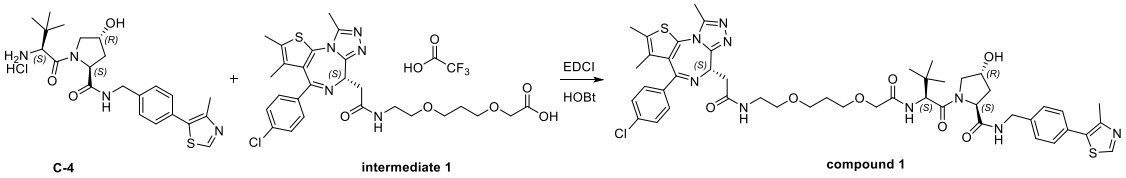

C-4 **intermediate 1** **compound 1**

To a solution of compound C-4 (50 mg, HCl salt), intermediate 1 (50 mg, 0.09 mmol), EDCI (27 mg, 0.14 mmol) and HOBt (19 mg, 0.14 mmol) in DMF (1.0 mL) was added DIPEA (0.05 mL, 0.27 mmol). The mixture was stirred at RT for 1 hour then purified by Reversed-phase chromatography (C18) (0.1% NH_4HCO_3 in water, 0-95% MeCN) to give compound 1 as a white solid (35 mg, yield: 43%).

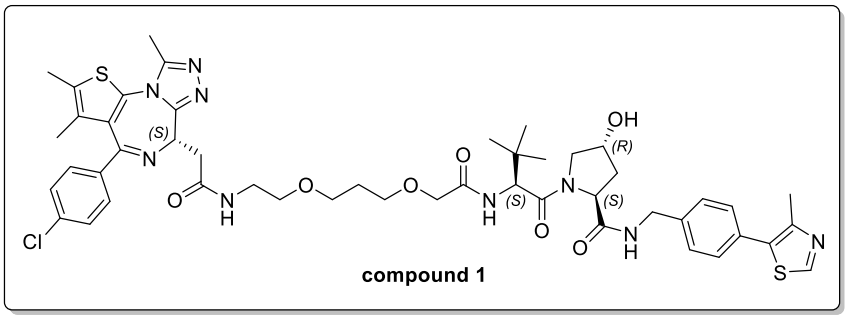

compound 1

LC/MS (ESI): m/z = 486.7 $[M+H]^+$ 1/2. RT = 1.74 min

^{1}H NMR (400 MHz, MeOD-*d*4) δ 8.88 (d, *J* = 6.5 Hz, 1H), 7.43 (ddd, *J* = 11.1, 9.8, 5.4 Hz, 8H), 4.74 – 4.33 (m, 6H), 4.07 – 3.78 (m, 4H), 3.75 – 3.54 (m, 6H), 3.45 (dt, *J* = 12.5, 7.4 Hz, 3H), 2.70 (s, 3H), 2.47 (t, *J* = 5.6 Hz, 6H), 2.30 – 1.85 (m, 4H), 1.71 (s, 3H), 1.04 (d, *J* = 8.8 Hz, 9H).

Synthesis of compound D-1

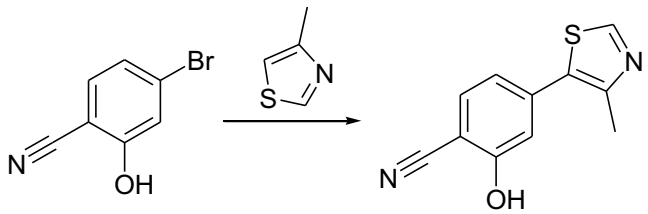

D **D-1**

A mixture of compound D (15.0 g, 76.1 mmol) in DMF (40 mL), then 4-methylthiazole (15.1 g, 152.2 mmol), palladium (II) acetate (853 mg, 3.80 mmol), and potassium acetate (14.9 g, 152.2 mmol) was added. The mixture was stirred at 90 °C under nitrogen for 18 hours. After cooling to ambient temperature, the reaction mixture was filtered. Fifty milliliters of water was added to the filtrate, and the resulting mixture was stirred at ambient temperature for 4 hours. The reaction mixture was filtered. The solid was collected by filtration and dried in an oven at 50 °C to afford compound D-1 as a yellow solid (12.3 g, yield: 75%).

Synthesis of compound D-2

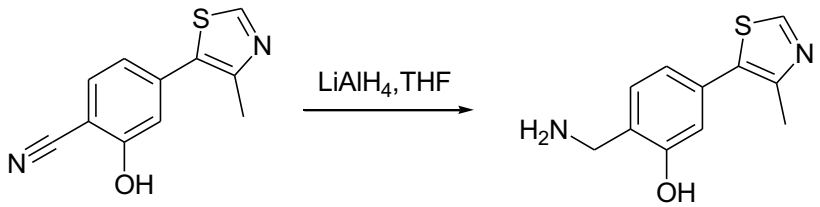

D-1 **D-2**

To a solution of compound D-1 (12.3 g, 56.9 mmol) in THF (60 mL) was added $LiAlH_4$ (1 M in THF, 142 mL, 142 mmol) at 0 °C. The reaction mixture was stirred at 50 °C for 30 min, and then THF (100 mL) and 15% NaOH (5.6 mL) was added at 0 °C. Na_2SO_4 was added to the mixture and the mixture was stirred at room temperature for 15 min. The slurry was filtered over a short pad of Celite and rinsed with THF (3 x 50 mL), and 20% MeOH in CH_2Cl_2 (3 x 50 mL), then the filtrate was concentrated under reduced pressure. The residue was purified by column chromatography on silica gel (0-10% MeOH/NH_3 in CH_2Cl_2) to give compound D-2 as a colorless oil (6.2 g, yield: 50%).

Synthesis of compound D-3

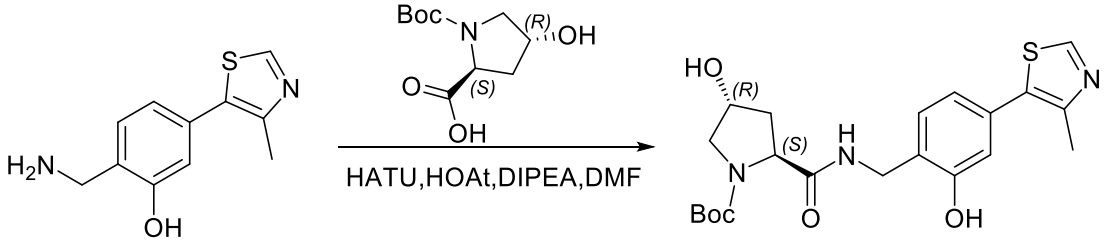

D-2 **D-3**

To a solution of compound D-2 (6.2 g, 28.2 mmol), (2S,4R)-1-(tert-Butoxycarbonyl)-4-hydroxypyrrolidine-2-carboxylic acid (6.5 g, 28.2 mmol), HATU (10.7 g, 28.2 mmol) and HOAt (3.8 g, 28.2 mmol) in DMF (20 mL) was added DIPEA (9.8 mL, 56.4 mmol) at 0 °C under N_2. The mixture was stirred at ambient temperature for 12 hours. TLC showed that the reaction was complete. The reaction mixture was quenched with H_2O (200 mL) and extracted with EtOAc (150 mL x 2). The combined organic layer was washed with brine (200 mL) and dried over Na_2SO_4. The organic solution was filtered and

concentrated. The residue was purified by column chromatography on silica gel (1-10 % MeOH in CH_2Cl_2) to afford the compound D-3 as white solid (8 g, yield: 65%).

Synthesis of compound D-4

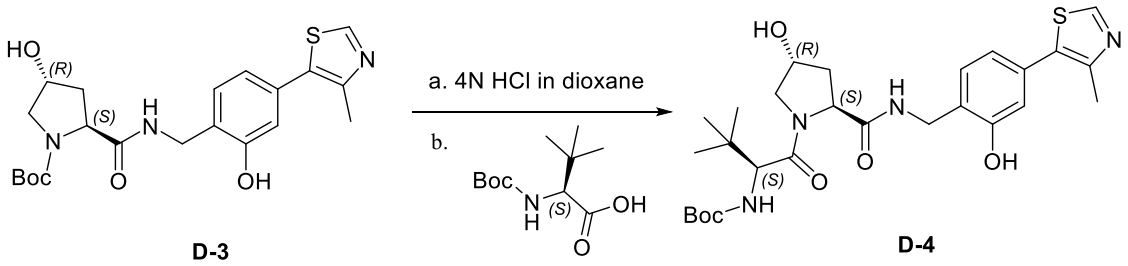

D-3 D-4

Compound D-3 (8.0 g, 18.5 mmol) was dissolved in 4 N HCl in dioxane (18 mL) and MeOH (18 mL), and the mixture was stirred at ambient temperature for 12 hours. The mixture was then concentrated, and the residue was dried under vacuum to afford the intermediate, HATU (10.5 g, 27.7 mmol) was added to a solution of this intermediate, (S)-2-((tert-butoxycarbonyl)amino)-3,3-dimethylbutanoic acid (4.3 g, 18.5 mmol), and DIPEA (9.6 mL, 55.5 mmol) in DMF (50 mL) at 0 °C under N_2. The mixture was stirred at ambient temperature for 12 hours when TLC showed that the reaction was complete. The reaction mixture was quenched with H_2O (200 mL) and extracted with EtOAc (150 mL x 2). The combined organic layer was washed with brine (100 mL) and dried over Na_2SO_4. The organic solution was filtered and concentrated. The residue was purified by silica gel flash column chromatography with DCM:MeOH (10:1) to afford the desired compound D-4 as an off-white solid (5 g, yield: 50%).

Synthesis of compound D-5

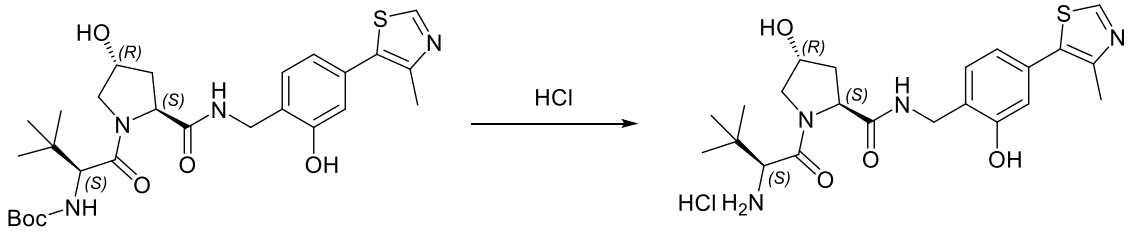

D-4 D-5

Compound D-4 (3.5 g, 6.4 mmol) was dissolved in 4 N HCl in dioxane (9.0 mL) and MeOH (9.0 mL), and the mixture was stirred at ambient temperature for 12 hours. The mixture was then concentrated and the residue was dried under vacuum to afford crude compound D-5 as an off-white solid, which was used in next step without further purification (4.0 g, HCl salt).

Synthesis of compound 1

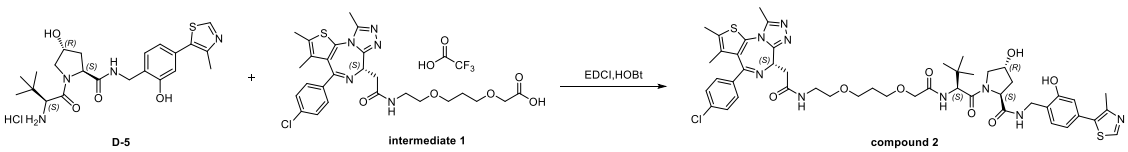

D-5 intermediate 1 compound 2

To a solution of compound D-5 (301 mg, HCl salt), intermediate 1 (350 mg, 0.52 mmol), EDCI (149 mg, 0.78 mmol) and HOBt (105 mg, 0.78 mmol) in DMF (8 mL) was added DIPEA (0.27 mL, 1.56 mmol). The mixture was stirred at RT for 1 hour, then purified by Reversed-phase chromatography (C18) (0.1% NH_4HCO_3 in water, 0-95% MeCN) to give compound 1 as a white solid (200 mg, yield: 39%).

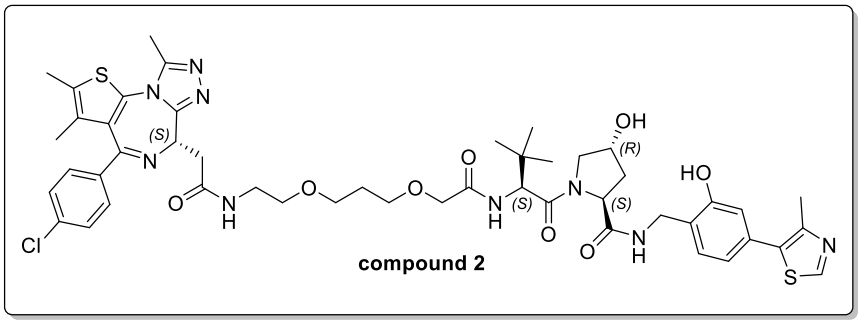

LC/MS (ESI): m/z = 494.7 $[M+H]^+$ 1/2. RT = 1.77 min

^{1}H NMR (400 MHz, MeOD-*d*4) δ 8.86 (d, *J* = 6.1 Hz, 1H), 7.62 – 7.20 (m, 5H), 7.00 – 6.82 (m, 2H), 4.81 – 4.25 (m, 6H), 3.99 (q, *J* = 15.4 Hz, 2H), 3.83 (dt, *J* = 11.1, 7.4 Hz, 2H), 3.70 – 3.55 (m, 6H), 3.53 – 3.40 (m, 3H), 2.71 (d, *J* = 4.6 Hz, 3H), 2.48 (t, *J* = 7.0 Hz, 6H), 2.27 – 2.06 (m, 2H), 1.91 (p, *J* = 6.2 Hz, 2H), 1.72 (d, *J* = 5.9 Hz, 3H), 1.10 – 0.95 (m, 9H).

Conjugation of VH032-based haptens

For the preparation of immunogens and screening compounds, VH032-based haptens (**1** (VHL-1), **2** (VHL-6), **3** (VHL-7), **4** (VHL-c)) were dissolved separately in conjugation buffer (0.1 M MES, 0.9 M NaCl, 0.02% sodium azide; pH 4.7) to a final concentration of 4 mg/mL and mixed either with a solution of 10 mg/mL keyhole limpet hemocyanin (KLH), 10 mg/mL cationic Bovine Serum Albumin (cBSA) or 7 mg/mL human Fc (fragment crystallizable) at a final protein/hapten molar ratio of 1:100. To this mixture, a 10 mg/mL aqueous solution of 1-ethyl-3-(3-dimethyllaminopropyl) carbodiimide (EDCI) was added (final protein-to-EDCI molar ratio 1:1750) and the reaction was incubated overnight. Reaction mixes were purified using Zeba Spin Desalting Columns that were pre-equilibrated in phosphate buffered saline (PBS, 0.137 M NaCl, 0.0027 M KCl, 0.01 M Na_2HPO_4, 0.0018 M KH_2PO_4, pH 7.4) (7K MWCO, Thermo Scientific). Protein concentrations were determined with Bradford reagent using unconjugated cBSA, KLH or human Fc as standards. The hapten/protein ratio for cBSA and human Fc conjugates was analyzed by MALDI-MS.

Methods

Immunization and cDNA preparation

Livestock farming and immunization of New World Camelids (llamas, alpacas, huarizos) was managed by Preclinics GmbH (Potsdam, Germany) according to national and international guidelines. The study was approved by an Institutional Animal Care and Use Committee, the Lower Saxony State Office for consumer protection and food safety (Oldenburg, Germany, reference number 33.19-42502-05-17A210). For generating an immune library, the three llamas (Lama glama) „Emma“, „Ferdinand“, and „Elvis“ were immunized subcutaneously with 300 µg mixed 1:1:1 VHL-1/-6/-7-carrier conjugate (100 µg of each VHL-carrier conjugate) in 0.5 mL PBS mixed with an equal volume of GERBU adjuvant S (GERBU Biotechnik GmbH, Heidelberg, Germany). Four weeks after priming, all animals received five boost immunizations identical to the prime injection in a two-week interval. For the immunization, KLH and cBSA were used alternatingly as carrier proteins for the VHL haptens, i. e. for injection 1, and 3 KLH conjugates and for injections 2, and 4 to 6 cBSA conjugates were used. In order to monitor the development of immune responses, serum samples were gained directly prior to prime immunization and on day 35, 49, and 77 of the immunization project. Four days after the sixth injection (day 88), a final blood sample was gained by venipuncture together with a final serum sample. Subsequently, peripheral blood mononuclear cells (PBMCs) were isolated by density gradient centrifugation on lymphocyte separation medium (LSM, Corning Inc., Corning, NY, USA) with a density of 1.077 to 1.080 g/mL at 20°C. The isolated cells from the interphase were collected and washed in DPBS (Corning). Finally, the cells were counted and lysed in RA1 buffer (Macherey-Nagel, Düren, Germany), 15 mM DTT and stored frozen until subsequent RNA and cDNA preparation. Humoral immune responses were monitored in diluted serum or plasma by ELISA on 96 well microtiter plates (high binding half area, Corning Inc., Corning, NY, USA) coated with VHL-1, VHL-7, or VHL-c human Fc conjugates and human IgG, respectively, as control. All proteins were diluted in 50 mM carbonate buffer pH 9.6 to a final concentration of 5 µg/mL. From each serum sample, a 1:4 serial dilution starting from 1:25 in PBS/BSA (1% w/v) was prepared. For detection of total IgG, dilutions starting from 1:100 were analyzed. Bound

total camelid IgG and heavy-chain IgG, respectively, was detected using peroxidase-conjugated monoclonal mouse-anti-llama IgG antibodies (produced in collaboration with University of Potsdam, PMID: 29475500, DOI: 10.1016/j.vetimm.2018.01.006), and 3,3',5,5'-tetramethylbenzidine (TMB One, Kementec, Taastrup, Denmark) as substrate. The absorbance at 450 nm and 620 nm reference wavelength was measured using a Mithras LB940 multimode reader (Berthold Technologies, Bad Wildbad, Germany). RNA was isolated from the lysed PBMCs using NucleoSpin RNA Midi kit for RNA purification (Macherey-Nagel, Düren, Germany) according to the manufacturer's instructions. The RNA was eluted in RNase-free water. For preparation of cDNA, RevertAid H Minus First Strand cDNA Synthesis Kit (K1632, Thermo Fisher Scientific Inc.) was used according to the manufacturer's instructions. For each animal, ten cDNA reactions using both oligo(dT)18 and random hexamer primers were used and pooled afterwards individually.

Generation of antibody phage libraries

The selection of VHL specific antibodies from a VHH antibody immune library generated from immunized llamas was managed by YUMAB GmbH (Braunschweig, Germany). Therefore, the cDNA pool was used for the amplification of the VHH gene sequences by PCR using proprietary gene specific primer pairs. In the first PCR, primers were used that bind to the leader peptide and CH2 region of the Llama Ig-heavy chain. Using gel extraction, gene sequences that are lacking the CH1 region were extracted and separated from gene amplicons that contain the CH1 domain. After purification, VHH genes were amplified in a second PCR. Here, the primers bind directly to the beginning and end of the VHH domain. Additionally, these primers contain a SapI restriction site, which allows Golden Gate cloning into YUMAB's phage display vector. As a result, the VHH will be genetically fused in-frame to a Myc- and HIS-tag and to a truncated pIII gene encoded on the vector backbone. The tagged VHH is separated from the pIII by a Trypsin cleavage site and an Amber stop codon. This allows Trypsin specific elution of antibody-phage during panning by cleaving the VHH part from the phage surface. Additionally, the Amber Stop codon allows soluble VHH production for screening purposes, when an amber suppressor E. coli strain is used. After purification of the amplified VHH gene sequences, cloning was done into YUMAB's antibody-phage display vector. For that purpose, the vector and VHH amplicons were mixed into a golden gate reaction, including T4 reaction buffer, T4 ligase and SapI. A total of 30 restriction and ligation cycles were performed. After heat inactivation for 20 min at 70°C, the ligation products were desalted using Amicon spin columns (30 K). The desalted DNA was mixed with ER2738 Electrocompetent Cells (Lucigen) and incubated for up to 5 min on ice, before electroporation was performed (1.7 kV pulse). The bacteria were recovered in SOC medium and incubated for 1 h at 37°C at 650 rpm. The size of the antibody-gene library was determined by serial dilution and colony counting of a sample of the recovered bacteria. For that purpose, the bacteria were serially diluted in LB medium and transferred onto 2YT agar plates, containing ampicillin (100 µg/mL) and glucose (0.1 M) (2YT-GA). After overnight incubation at 37°C, the number of colonies was counted visually, and the total number of recovered clones calculated. Additionally, the single clones were used for determination of the VHH insert-rate by cPCR and the number of clones with a functional ORF determined by DNA-sequence analysis. Simultaneously, the remaining recovered bacteria were incubated in 2YT-GA and incubated at 37°C and 250 rpm until an OD600 of 0.5 was reached. A sample of the culture was extracted, and bacteria were infected with M13K07 helper-phage (MOI of 20) for 30 min at 37°C. After another propagation cycle for 30 min at 37°C and 250 rpm, the infected bacteria were pelleted by centrifugation at ~3000 g for 10 min. For the production of antibody-phage particles, the bacteria were resuspended in glucose-free 2YT medium, containing Ampicillin (100 µg/mL) and Kanamycin (50 µg/mL) (2YT-AK). The cultivation was continued for 16 h at 30°C. For the purification of the antibody-phage particles, the culture was centrifuged for 40 min at ~3000 g to separate the bacteria from the antibody-phage containing culture supernatant. Then, PEG/NaCl precipitation of the antibody-phage particles was performed, followed by centrifugation (1 h at ~3000 g) and resuspension of the pelleted antibody-phage in phage-dilution buffer. The phage preparation was polished with a high-speed centrifugation step (2 min at ~16000 g). The supernatant was recovered and used for antibody-phage selection. After purification of the antibody-phage particles, the phage concentration was determined. For that purpose, the phages were serially diluted in LB medium and used for the infection of E. coli (30 min at 37°C). The infected bacteria were transferred onto 2YT agar plates, containing ampicillin (100 µg/mL) and glucose (0.1 M) (2YT-GA). After overnight incubation at 37°C, the number of colonies was counted visually, and the concentration of colony forming units calculated. The size of the antibody phage library added up to a diversity of 1.44×10^9 colony forming units. In addition, the insert-rate was determined by colony PCR and the number of clones with a functional ORF determined by DNA-sequence analysis. Additionally, the presence of an antibody-pIII fusion protein was checked by SDS-PAGE, western blotting and anti-pIII immunoblot staining of the antibody-phage particles.

Phage display and library screening

Phage display and screening was conducted at Yumab GmbH, Germany. First, the library was cleared from unspecific or cross-reactive antibody-phages. For that purpose, antibody-phage particles (50-100 x fold excess of the library diversity) were diluted in 2% BSA solution, containing 0.05% Tween20 (2% BSA-PBST) and incubated first in Streptavidin-coated ELISA plates (coated with 10 µg/mL, 200 µL/well) for 1 h at RT, followed by incubation with magnetic Streptavidin beads (Dynabeads, Thermo Scientific, 50 µL) for at least 1 h at RT under rotation. Antibody-phages that bound to the negative antigens were removed from further selection by isolation of the phage-containing supernatant. After that, the cleared library was selected for target antigen specific antibodies. For that purpose, a conjugate of the von Hippel-Lindau (VHL)-recruiting ligand and a PEGylated crosslinker with pendant amine was acquired ((S,R,S)-AHPC-PEG_3-NH_2 hydrochloride Sigma-Aldrich, 901511-50MG) and biotinylated via Biotin-NHS-ester coupling. The biotinylated VHL ligand was purified and analyzed by HPLC. First, the biotinylated VHL ligand (50 nM) was added to the cleared library. Antibody-phages that bound to the biotinylated target antigen were captured and recovered from the solution using magnetic streptavidin beads (Dynabeads, Thermo Scientific, 50 µL). The beads were washed three times with a 2% BSA-PBST solution and twice in PBS in order to remove unspecific or weakly bound antibody-phage particles. Antigen-specific antibody phages were eluted from the beads by Trypsin (10 µg/mL) treatment at 37°C for 30 min. The eluted phages were rescued by infection of E. coli (OD600 = 0.5) in 2YT medium for 30 min at 37°C. After propagation for 30 min at 37°C and 650 rpm, infected bacteria were selected by addition of glucose (0.1 M) and ampicillin (10 µg/mL). The cultivation was continued for 30 min at 650 rpm and 37°C before M13K07 helper phage was added (MOI 1:20). The co-infection with helper phage was performed for 30 min at 37°C, followed by incubation for 30 min at 37°C and 650 rpm. For the amplification of antibody-phage particles, the bacteria were pelleted by centrifugation (~3000 g, 10 min) and the culture medium exchanged to glucose-free 2YT-AK before the cultivation was continued for 16 h at 30°C and 650 rpm. The amplified phages were used for two more selection cycles as described above. To identify the best performing antibody variants targeting VH032 (**5**). The selection outputs of rounds three and four were subjected to single clone analyses. After the antibody-phage selection, the binding characteristics of the monoclonal antibody clones were analyzed. 384 single clones were selected from the selection output after panning round two and three and used for VHH antibody expression in bacteria. For that purpose, eluted phages were used for infection of E. coli (as described above) and cultivated on 2YT-GA agar plates. The plates were incubated at 37°C until single colonies were observed. The single colonies were picked and transferred into microtiter plates containing 2YT-GA culture medium and cultivated at 37°C and 250 rpm for 16 h. For VHH production, 15 µL of each overnight culture was transferred to microtiter plates containing 2YT-A and 50 µM IPTG. Antibody production was done for 16 h at 30°C and 250 rpm. Each antibody production was tested for their binding specificity by ELISA on Streptavidin + biotinylated VHL ligand, Streptavidin, Human Fc-VHL-1, and Human Fc. For that purpose, 384-well ELISA plates were either coated with Streptavidin (40 ng/well), followed by blocking with 2% BSA-PBST solution and capturing of the biotinylated antigen (20 ng/well), or by direct immobilization of the non-biotinylated antigen (20 ng/well), followed by blocking with 2% BSA-PBST. The antibody-containing E. coli productions were mixed with 2% BSA-PBST in a 1:1 ratio, transferred to the washed ELISA plates (30 µL/well) and incubated for 1 h at RT. After washing, bound antibodies were detected via a secondary anti-Myc HRP conjugated antibody. After washing, binding was quantified by standard TMB staining and absorbance reading. Antibody clones were identified as antigen specific, if the ELISA binding signal to the positive antigens was ≥ 0.1, the ELISA binding signal to the negative antigens was ≤ 0.1, and the S/N ratio between positive and negative antigens was ≥ 10. 562 Hits were identified from the llama library. All Hits were used for DNA-sequence analysis to identify antibodies with a unique antibody sequence (≥ 1 amino acid difference in the CDRs). 113 unique clones were identified from the llama library. To identify clones with the best binding affinity, a biolayer interferometry (BLI) off-rate measurement was performed. First, VHH containing culture supernatants were produced of the unique clones. After that, the association and dissociation of the antibody fragment to the biotinylated VHL was measured which was immobilized onto BLI Streptavidin sensors. The binding curve was fitted with a 1:1 binding model and the dissociation rate calculated. Based on the off-rates and antibody sequence information, 10 lead clones (named MIC5 – MIC14) were selected for conversion into the final antibody format.

Reformatting of VH032-binding VHH domains into PROxAb Shuttles

Reformatting was conducted at Yumab GmbH, Germany. For this, the VHH genes were amplified from the phagemid DNA by PCR and cloned into two different IgG expression vectors. These expression vectors encoded the therapeutic anti-CD33 antibody gemtuzumab bearing a receptor-silenced human IgG4 PG-SPLE or human IgG1 PG-LALA (only for Shuttles with humanized VHHs) backbone (αCD33)[3], the epidermal growth factor receptor-targeting (EGFR) antibody cetuximab bearing a receptor-silenced

human IgG1 PG-LALA backbone (αEGFR) or an antibody targeting digoxigenin bearing either the above-mentioned receptor silenced human IgG4 or IgG1 backbone (αDIG). For vector generation, the individual VHH antibody fragments were genetically fused to the C-terminus of the IgG antibody heavy chains. The VHH domain was separated from the IgG heavy chain via a short glycine-serine amino acid linker (GSGGGSGGSGGGGSG). After sequence verification and preparation of transfection-grade DNA, human embryonic kidney (HEK) cells were transiently transfected with the expression vectors and incubated for 7 days at 37°C and 5% CO_2 to enable production of the final PROxAb Shuttle antibodies. The cells were separated from the antibody supernatant by centrifugation at 3000 rpm for 20 minutes at 4°C and purified using protein A affinity chromatography. After clearance of the culture supernatant from cells by centrifugation, the IgG antibodies were purified by Protein A affinity chromatography. After adjustment of the buffer to PBS, the protein concentration of the antibodies was determined by UV/VIS spectrometry. Integrity and purity of the antibodies were assessed by SDS-PAGE under reducing conditions. The functional binding activity of the antibodies to the target antigen was measured by ELISA.

***In vitro* characterization of VH032-binding VHH antibody domains**

The kinetic and affinity parameters of the VHH/PROTAC interactions were evaluated by surface plasmon resonance (SPR). αCD33xMIC7, αEGFRxMIC7 or αCD33xhMIC7_1.6 were immobilized onto a high-capacity amine sensor chip (Bruker Daltonics) via the standard amine coupling procedure, at 25 °C. Prior to immobilization, the carboxymethylated surface of the chip was activated with 200 mM 1-ethyl-3-(3-dimethylaminopropyl)-carbodiimide and 25 mM N-hydroxy succinimide (NHS) for 10 min. The PROxAb variants were diluted to 10 µg/mL in 10 mM acetate at pH 4.5 and immobilized on the activated surface chip for 7 min, in order to reach 3,000 to 9,000 response units (RU). The remaining activated carboxymethylated groups were blocked with 1 M ethanolamine pH 8 in a 7 min injection step. HBS-N, which consists of 10 mM HEPES pH 7.4 and 150 mM NaCl, was used as the background buffer during immobilization. PROTACs were prediluted in DMSO, diluted 1:50 in running buffer (12 mM phosphate, pH 7.4, 137 mM NaCl, 2.7 mM KCl, 0.05% Tween20, 2% DMSO) and injected at 10 different concentrations using two-fold dilution series, from 1 µM to 0.002 µM. A DMSO solvent correction (1% - 3%) was performed to account for variations in bulk signal and to achieve high-quality data. Interaction analysis cycles consisted of a 300 sec sample injection (30 µL/min; association phase) followed by 900 sec of buffer flow (dissociation phase). All sensorgrams were processed by first subtracting the binding response recorded from the control surface (reference flow-channel), followed by subtraction of the buffer blank injection from the active flow-channel (target protein immobilized). All datasets were fit to a simple 1:1 Langmuir interaction model to determine the kinetic rate constants. The experiments were performed on a SPR-32 PRO (Bruker Daltonics, Bremen, Germany) at 25°C or 37°C and the interactions were evaluated using the provided Sierra Analyser Software (version 3.4.5.).

Generation of PROTAC-complexed PROxAb Shuttles

Complexation to create PROTAC-complexed PROxAb Shuttles was performed as follows: 10 µM (final) antibody-VHH fusion were mixed in PBS pH 7.4 with varying equivalents of VHL-based PROTAC in DMSO to achieve the desired loading. PROxAb Shuttles determined for *in vivo* application were complexed at an antibody concentration of 6 mg/mL. For *in vitro* application, Tween-20 was typically added to a final concentration of 0.3% in order to use a Tecan D300e dispenser for PROxAb Shuttle application on cells. The samples were incubated on a ThermoMixer for 3 h at 25°C while shaking at 650 rpm. Note, 3 h incubation was chosen to assure full loading. However, we observed full complexation within minutes (data not shown). No aqueous Tween-20 was added for complex investigation using size-exclusion chromatography, flow cytometric analysis or native SEC-native MS.

Isothermal titration calorimetry

ITC measurements were performed with VP-ITC microcalorimeter from MicroCal/Malvern Panalytical (UK). PROxAb Shuttles, His-tagged MIC7-VHH and the respective VHL-ligand compounds were formulated in 30 mM HEPES; 150 mM NaCl; pH 7.4 with optional addition of 0.01% Tween-20 for all titration experiments. The proteins were loaded into the injection syringe with final concentrations of 25 µM for Shuttles and to 50 µM for VHH. VH032 stock solutions of 10 mM in DMSO were diluted to 5 µM concentrations with buffer and loaded into the sample cell. All buffers were adjusted to a final concentration of 1% (v/v) DMSO. Both, the titrate and titrant solutions were degassed prior to loading the calorimeter cell and injection syringe. ITC titrations were conducted at a constant temperature of 303 K. ITC data analysis was performed using the Origin 7-based (OriginLab Cooperation Northampton, USA) calorimetry customization supplied as standard instrument software by MicroCal / Malvern Panalytical (UK). The integrated heat data were fitted with a one-site binding model to determine the

apparent values for affinity, enthalpy, and stoichiometry of binding. Binding parameters of reference ligands were monitored, and the binding stoichiometry was employed as reference point for normalizing the concentration of different protein batches.

Native size exclusion liquid chromatography – native Mass spectrometry analysis

An eksigent M5 MicroLC system from SCIEX (ON, Canada) connected to a quadrupole time of flight (QTOF) mass spectrometer (MS) (QTOF X500B, SCIEX, ON, Canada) was used for the analysis. The protein samples were separated using a PolyHYDROXYETHYL A capillary (150 x 0.30 mm, 3 µm, 1000 A). The column temperature was set to 25°C and an isocratic gradient with 100 mM ammonium acetate pH 6.8 was run with 10 µL/min for 10 min. A positive time of flight (TOF) MS method was used for analysis. The electrospray voltage of the X500B QTOF instrument was set to 5500 V and the temperature was 400 °C. Full MS scans were acquired over a mass to charge range of 5000 - 7000 with an accumulation time of 1 sec and time bins to sum 120. The ion source 1 and 2 gases were set to 60 psi. The declustering potential was set to a value of 20 V. The data was evaluated manually using the Explorer tool of the SCIEX OS software, version 1.5.0.23389. For this purpose, a suitable time range of the eluting peak in the total ion current chromatogram (TIC) was summed to obtain a multiply charged spectrum. The 5 most intense multiple charge peaks were marked and deconvoluted using the Bio Tool Kit in the Explorer. The input spectrum isotope resolution was set to 1000 (very low). The mass step was 1 Da and the charge agent was set to H+. The mass range to be calculated was set between 170000 and 190000 Da.

Flow cytometric analysis of PROxAb Shuttle binding to CD33 cell surface receptors

Flow cytometric analyses were conducted at Reaction Biology Europe GmbH, Germany. For this, αCD33xMIC7 and αDIGxMIC7 were complexed with GNE987 (**6**) in different ratios resulting in different PROTAC-to-antibody-ratios as stated in the chapter "Generation of PROTAC-complexed PROxAb Shuttles". Non-complexed PROxAb Shuttles and the control antibody, gemtuzumab with IgG4 PG-SPLE mutation (αCD33), were treated with the same procedure exchanging the DMSO dissolved PROTAC to DMSO only. Subsequently, the control antibody, complexed and non-complexed PROxAb Shuttles were stored at 4 °C overnight. On the next day, the control antibody, complexed and non-complexed PROxAb Shuttles were diluted in FACS-buffer (PBS 2% FCS 1 mM EDTA) at 1:100 (100 nM final antibody concentration, accordingly) and 1:1000 (10 nM final antibody concentration, accordingly) immediately before addition to cells. Cell lines (MV4-11, MOLM-13 and RAMOS) were pre-cultured for about 1 week in RPMI+Glutamax (Gibco) + 10% FCS (Bio&SELL) + 1% Penicillin/Streptomycin (Gibco). On the day of staining, cells were counted and plated at $2.0x10^5$ cells per well in clear v-bottom 96-well microtiter plates (Thermofisher). Cells were spun down in the 96-well plate at 300xg for 5 min at 4 °C, supernatant was poured off, cell pellets were loosened by vortexing, and 100 µL PBS (Gibco) were added per well to wash cells. After centrifugation as before, PBS was poured off, and 100 µL of pre-diluted control antibody, complexed and non-complexed PROxAb Shuttles (1:100 and 1:1000) was added per well. Plates were sealed, vortexed, and staining incubation was performed for 1 h at 4 °C. Thereafter, 100 µL FACS-buffer was added per well, followed by centrifugation, pouring off of supernatant, vortexing and again addition of 100 µL FACS-buffer. After centrifugation as before, FACS-buffer was poured off, and 100 µL secondary antibody (goat anti-human FITC, Jackson, #109-095-098) was added per well at 1:100 dilution in FACS-buffer. Plates were sealed, vortexed, and staining incubation was performed for 1 h at 4 °C. Cells were washed as described above and finally resuspended in 100 µL FACS buffer prior to flow cytometric measurement using a CytoFLEX S flow cytometer (Beckman Coulter). 10.000 events were recorded per sample and subsequently analyzed using FlowJo software. For the analysis, mean fluorescence intensity (MFI) of the FITC-channel was assessed in single live cells, MFI of secondary antibody only samples were subtracted from all samples, duplicate samples were averaged and plotted using GraphPad prism.

Flow cytometric analysis of PROxAb shuttle internalization

Flow cytometric analyses were conducted at Reaction Biology Europe GmbH, Germany. The αCD33xMIC7 PROxAb variant was incubated for 2 h at 25 °C and 650 rpm in PBS with 5% VH032-pHAb dye (**15**) (dissolved in DMSO, Figure 3) at a 1.8-fold molar excess. The procedure was performed under the exclusion of light. CD33-positive MOLM13, MV4-11, U937 and receptor negative RAMOS cells were cultured in RPMI-1640 with 10% FCS. From each cell line, 200,000 cells were harvested, centrifuged, and incubated with either the dye-complexed PROxAb Shuttle or the dye-only control in 200 µL PBS with 1% FCS at a final concentration of 10 µg/mL. 6 h incubations were performed at 37 °C while shaking at 650 rpm in the dark. The cells were washed once with PBS containing 1% FCS and subsequently resuspended in 400 µL PBS with 1% FCS. Flowcytometric analyses were performed on a Becton Dickinson FACSCalibur flow cytometer. Staining of dead cells with propidium iodine (PI) was

not performed to omit possible interference with VH032-pHAb dye (**15**). Quantitative analyses were done using the software FlowJo from BD Biosciences.

Assessment of BRD4 degradation via western blotting

Western Blotting was performed at Reaction Biology Europe GmbH, Germany. For degradation assays, CD33-positive MV4-11 cells were treated with GNE987-complexed αCD33 or αDIG PROxAb Shuttles at 1, 0.1, 0.01 and 0.001 nM. Unbound GNE987 (**6**) was used as a control at a concentration of 1 nM. MV4-11 cells were cultured in RPMI-1640 medium supplemented with 10% FCS and penicillin as well as streptomycin. MV4-11 cells were seeded in 12-well plates at 1 million cells/mL in 2 mL culture medium and cultured overnight at 37 °C and 5% CO_2. PROxAb Shuttle complexation with PROTAC was performed as described previously. A control comprising unbound GNE987 (**6**) was preincubated at identical conditions, but in absence of a PROxAb Shuttle. Subsequently, cells were treated with either GNE987 (**6**)-complexed αCD33 or αDIG PROxAb shuttle at a PROTAC-to-antibody ratio of 1:1 or with GNE987 (**6**) using a Tecan D300e dispenser. All tested conditions were normalized to 0.0005% (v/v) DMSO and $3.x10^{-5}$ % (v/v) Tween-20. The cells were subsequently incubated at 37 °C and 5% CO_2 for 24 h. Treated cells were harvested, washed in PBS and the resulting cell pellets were lysed in cell lysis buffer (20 mM TRIS pH 7.4, 100 mM NaCl, 1 mM EDTA, 0.5% TritonX-100) supplemented with Roche cOmplete protease inhibitor mixture. After incubation for 10 min on ice, crude lysates were collected via centrifugation at 15,000xg, 4 °C and the resulting supernatants were precipitated by acetone. Dried pellets were dissolved in SDS loading buffer and the protein concentrations were determined with a Mettler Toledo UV5Nano photometer. Subsequently, samples (50 µg/lane) were applied to 4-12% Bis-Tris SDS-PAGE gels (Thermo Fisher Scientific). After completion of the SDS run, the samples were transferred onto nitrocellulose membranes (Sigma Aldrich) via western blotting. Next, membranes were blocked with 5% skim milk in 0.1% TBS-Tween-20 and incubated with primary antibodies against BRD4 (CST#13440, rabbit, 1:1000, Cell Signaling Technology) and Actin (PQ#679, mouse, 1:10,000, ThermoFisher) in 5% skim milk and 0.1% TBS-Tween-20. After incubation with corresponding HRP-labeled anti-rabbit/mouse secondary antibodies (GE-Healthcare) at 1:10,000 dilution, the blots were developed with ECL solution (Advansta) and x-ray films (GE-Healthcare). Afterwards, the obtained results were analyzed with the software ImageJ (version 1.53K, NIH). Background subtracted BRD4 signals were normalized to corresponding actin signals and the normalized BRD4 signal of the solvent control served as the reference point for the 100% value.

***In vitro* cytotoxicity assays**

Cell viability assays were performed at Reaction Biology Europe GmbH, Germany. Therefore, cancer cells were seeded in different media into white cell culture-treated flat and clear bottom multi-well plates (corning®), followed by overnight incubation in a humid chamber at 37 °C and 5% CO_2. PROxAb Shuttle complexation with PROTAC was conducted as described previously. Serial dilutions of PROxAb Shuttle solutions were added to the cells using nanodrop dispensing and a Tecan D300e Digital Dispenser. All wells were normalized to the same volume using solutions of 0.3% Tween-20 in PBS, pH 7.4 and DMSO to a final concentration of 0.05% DMSO and 0.003% Tween-20. Subsequently, treated cells were incubated at 37 °C and 5% CO_2. The assays were developed after 3 days using CellTiter-Glo Luminescent Cell Viability Assay as described in the manufacturer's protocol. In brief, the plates were equilibrated to room temperature for 30 minutes. Afterwards, 100 mL CellTiter-Glo Buffer were added to the CellTiter-Glo Substrate Flask and mixed well. Next, 25 µL of the reagent were transferred to each well of the cell culture plate. After incubation for 3 minutes at room temperature and shaking at 550 rpm, the plates were incubated for another 30 minutes at room temperature. The luminescence signals were measured on an Envision reader from Perkin Elmer. Solvent alone and staurosporine (at 10 µM) served as 100% viability and 0% viability controls, respectively. Raw data were converted into percent cell viability relative to solvent and staurosporine, which were set to 100% and 0% viability, respectively. IC50 value calculations were performed using GraphPad Prism software with a variable slope sigmoidal response fitting model.

***In vivo* pharmacokinetic studies**

In preparation for the *in vivo* pharmacokinetic studies, αCD33 and αEGFR PROxAb Shuttles were complexed with the PROTAC GNE987 (**6**) or GNE987P (**7**) (αCD33 PROxAb Shuttle only) at a PROTAC-to-antibody ratio of 2:1, as described previously.

αCD33 antibody, αCD33xMIC5, αCD33xMIC5 complexed with GNE987, αCD33xMIC7, αCD33xMIC7 complexed with GNE987

Studies were performed in C57BL/6N inbred mice (n = 2 males and females for each group) that were provided by Charles River Laboratories Italia, Calco, Italy. The 7 – 8-week-old mice received 30 mg/kg

(corresponding to 0.38 mg/kg PROTAC) of non-complexed and complexed αCD33xMIC5 and αCD33xMIC7 PROxAb Shuttles as well as αCD33 antibody as single doses that were intravenously injected into the tail vein. Blood samples were serially collected from all animals using a microsampling technique (20 µL for each blood withdrawal). After administration, 2 blood samples were taken on the first day and another 7 were taken during the following 3 weeks. Each sample was collected in a pre-chilled (0-4 °C) Minivette POCT EDTA tube, transferred in Microvette CB300 EDTA and centrifuged at 2500 x g for 10 min at 4 °C. The obtained plasma was transferred into a new vial and immediately stored at -80 °C until further analyses. The PK study as well as animal handling and experimentation were conducted in accordance with the Italian D.Lvo. 2014/26 and Directive 2010/63/EU. The study was performed at the Instituto di Ricerche Biomediche Antoine Marxer, Colleretto Giacosa, Italy. The institute is fully authorized by the Italian Ministry of Health. The total antibody concentration was determined by ligand binding assays (LBA) based on the Meso Scale Diagnostics technology (MSD, LLC., Rockville, MD). All incubation steps were performed at 22 °C with gentle agitation. All washing steps (200 µL/well) were performed with PBS-T, containing PBS, pH 7.4 and 0.01% Tween-20, using the plate washer ELx405 (BioTek instruments Inc., Winooski, VT). First, 2.5 µg/mL biotin-SP-conjugated AffiniPure goat anti-human IgG, Fcγ fragment specific (Jackson ImmunoResearch Europe Ltd., JIR, Cambridgeshire, United Kingdom, #109-065-098) was coated on MSD GOLD 96-well Streptavidin QUICKPLEX Plates (MSD, #L55SA) for 2 h. Afterwards, the plates were washed three times. Plasma samples, standards and quality controls were serially diluted in dilution buffer, consisting of PBS, pH 7.4, 0.05% Tween-20 and 3.0% (w/v) BSA, and incubated for 1 h. The plates were washed again and incubated for another hour with 0.6 µg/mL mouse anti-human IgG, F(ab')2 fragment specific (JIR, #209-005-097), previously labeled with MSD GOLD SULFO-TAG (MSD, #R31AA-1) according to the manufacturer's procedure. After a final washing step, 150 µL of 2x MSD Read Buffer T with surfactant (MSD, #R92TC) was added to each well and plates were read on a MESO Quickplex SQ120 plate reader (MSD). The Software Watson LIMS (Version 7.5, ThermoFisher Scientific Inc.) was used to fit the standard curve with a 5PL (Marquart) equation, weighting factor $1/Y^2$, and to calculate the total antibody (tAntibody) concentration of the plasma samples. The lower limit of quantification (LLOQ) of the method was 50 ng/mL. The concentration of GNE987 (**6**) was determined by liquid chromatography tandem mass spectrometry (LC-MS/MS) using a SCIEX 5500 triple quadrupole with Turbo Ion Spray source (ITS) in positive modality (SCIEX, Redwood City, CA, USA). Chromatographic separation was achieved using a Waters ACQUITY UPLC BEH (C18, 2.1 x 50 mm, 1.7 µm) column, mounted in a Waters ACQUITY I-class UPLC system (Milford, MA, USA), configured with a 100 µL extension loop. The chromatographic gradient used for phase A (H_2O:acetonitrile 95:5, 0.1% formic acid) and B (acetonitrile:H_2O 95:5, 0.1% formic acid) at a flow rate of 0.350 mL/min, was 0.25 min of 100% A isocratic, followed by a 2.25 min gradient to 100% B, with a subsequent 0.75 min of washing step at 100% B and 2.5 min of reconditioning at initial conditions. Extraction of GNE987 (**6**) from C57BL/6N mouse plasma samples was carried out by protein precipitation technique. In that manner, 3 µL of plasma sample were precipitated in 100 µL of acetonitrile containing 0.5 ng/mL of Exatecane-d5, used as internal standard, on a Phenomenex Impact Protein Precipitation Plate (Phenomenex, Torrance, CA, USA, CE0-7565). After 5 min of shaking at 900 rpm, all the wells were filtered by vacuum and collected in a clean 96-well plate. Subsequently, they were diluted with 100 µL of an aqueous solution containing 2.5% formic acid and submitted to LC-MS/MS analyses. All reagents were LC-MS grade or equivalent. The Software Watson LIMS (Version 7.5, ThermoFisher Scientific Inc.) was used to fit the standard curve on the area ratio (analyte signal/internal standard signal) on a linear regression, weighting factor $1/X^2$, and to calculate the total GNE987 PROTAC (**6**) concentration of the plasma samples. The lower limit of quantification (LLOQ) was 5 ng/mL, and the complete range of quantitation was 5-2000 ng/mL. The main pharmacokinetic parameters were estimated by noncompartmental analysis (NCA) using Phoenix WinNonlin version 8.3.4 (Pharsight Corporation, USA). The pharmacokinetic parameters have been obtained or calculated from the individual plasma concentrations of total antibody and GNE987 (**6**) analyte versus time after administration. Individual plasma concentration-time profiles were used for parameter estimation. The concentration of all pharmacokinetic samples that were calculated to be below the quantification limit (BQL) were considered as missing value to better estimate $AUC_{0\text{-}inf}$, clearance and volume of distribution. The values for the terminal half-life ($t_{1/2}$) and the first order rate constant associated with the terminal log-linear portion of the curve (ʎz) were calculated only when at least 3 time points were quantifiable in the terminal phase of the linear regression. Values below the quantification limit were considered 0 ng/mL for descriptive statistics.

αCD33xMIC7+ GNE987P, αCD33xMIC7+ GNE987P administered sequentially and GNE987P alone
The pharmacokinetic studies of αCD33xMIC7 complexed with GNE987P (**7**), αCD33xMIC7 and GNE987P (**7**) administered sequentially, as well as of GNE987P (**7**) alone were performed at EMD

Serono Research & Development Institute, Inc. Billerica and are described in the following. All parts of the study plan concerning animal care have been reviewed by the EMD Serono Billerica site "Institutional Animal Care and Use Committee (IACUC)" which reports to the EMD Serono Billerica site Head. Protection of animals used, housing and welfare are guaranteed according to the Protocol number 20-002: Pharmacokinetic Studies in Rodents, Principal Investigator: Mary-Jo Miller. Physical facilities for accommodation and care of animals are in accordance with the provisions of the AAALAC (Association for Assessment and Accreditation of Laboratory Animal Care) and the EMD Serono animal facility is recorded as AAALAC unit #001473. For GNE987P (**7**) alone, female C57BL/6N inbred mice (composite profile, n=9) provided from Taconic (NY, USA) received a single tail vein intravenous (i.v.) bolus injection of 0.30 mg/kg in 2% (v/v) DMSO / 20% (v/v) (hydroxypropyl ß-cyclodextrin) Kleptose in water, at a dosing volume of 5 mL/kg. For the αCD33xMIC7 PROxAb Shuttle complexed with GNE987P (**7**), C57BL/6N inbred mice (n=12, composite profile) provided from Taconic (NY, USA) received a single tail vein intravenous (i.v.) bolus injection of 30 mg/kg of complexed αCD33xMIC7 PROxAb Shuttle (corresponding to 0.38 mg/kg PROTAC) in 5% (v/v) DMSO in PBS, at a dosing volume of 5 mL/kg. The last group was administered sequentially, first with the non-complexed αCD33xMIC7 PROxAb Shuttle at the same dose as in the group treated with the PROxAb Shuttle complex, followed 24h later by the PROTAC (GNE987P (**7**)) in the corresponding dose used for the αCD33xMIC7 PROxAb Shuttle complexed with GNE987P (**7**). For this, female C57BL/6N inbred mice (composite profile, n=12) provided from Taconic (NY, USA) received a single tail vein intravenous (i.v.) bolus injection of the αCD33xMIC7 PROxAb Shuttle of 30 mg/kg in 5% (v/v) DMSO in PBS, at a dosing volume of 5 mL/kg. The same mice, 24h after the administration of the PROxAb Shuttle, received a single tail vein intravenous (i.v.) bolus injection of GNE987P (**7**) at 0.40 mg/kg in 2% (v/v) DMSO/20% (v/v) (hydroxypropyl ß-cyclodextrin) Kleptose in water, at a dosing volume of 5 mL/kg. For the GNE987P (**7**) alone, consecutive blood samples (25 µL) were taken sub-lingually under light isoflurane anesthesia (n=3 per group (G)) at 0.1 (G1), 2 (G2), 6 (G3), 24 (G1), 72 (G2), 120 (G3), 240 (G2), 336 (G3) and 360h (G1) on K3-EDTA in pre-chilled Eppendorf tubes, stored on ice for at least 15 min before centrifugation at 2500 x g for 10 min at 4°C to obtain plasma. For the αCD33xMIC7 PROxAb Shuttle complexed with GNE987P (**7**) or the group administered sequentially with the αCD33xMIC7 PROxAb Shuttle followed by the PROTAC GNE987P (**7**), consecutive blood samples (25 µL) were taken sub-lingually under light isoflurane anesthesia (n=3 per group (G)) at 0.1 (G1), 6 (G2), 24 (G3), 96 (G4), 168 (G1), 240 (G2), 360 (G3), 600 (G4), 840 (G1), 960 (G2), 1080 (G3) and 1200h (G4) on K3-EDTA in pre-chilled Eppendorf tubes, stored on ice for at least 15 min before centrifugation at 2500 x g for 10 min at 4°C to obtain plasma. For the sample preparation, 10 µL plasma was diluted with 10 µL of methanol and precipitated with 80 µL of acetonitrile, containing labetalol as internal standard (2.5 µg/mL), in LowBind® (protein) plates. After shaking/vortexing for 1 min, samples were filtered, (Captiva filtration on polypropylene filter, 0.45 µm pore size) and 120 µL of methanol:water (1:1, v/v) was added to the filtrate and stored at 4°C until analysis and put in the autosampler before injection. The analysis was carried out on a LC-MS/MS system consisting of an UPLC coupled to a QTRAP 6500+ (Sciex) mass spectrometer. Mobile phase A was water with 0.1% formic acid and mobile phase B was methanol with 0.1% formic acid. The gradient was started with 10% B to 95% B in 1.5 min and maintained at 95% B for 2 min, then decreased to 10% B in 0.5min and maintained to 10% B for 2 min. The chromatography was performed on a Poroshell 120 EC-C18 column, 2.7 µm particles, 3 x 50 mm, from Agilent Technologies. The flow rate was 0.6 mL/min and the cycle time (injection to injection) was approximately 6 minutes The sample injection volume was 10 µL. MRM transition for GNE987P (**7**) was 551.669 (m/z, z = 2) $\rightarrow$ 318.1 (m/z, z=2) and 329.101 (m/z, z=1) $\rightarrow$ 91 (m/z, z=1) for labetalol (IS). The calibration curve for quantitation was based on standards ranging from 0.5 (Lower Limit of Quantitation) to 10000 (Upper Limit of Quantitation) ng/mL, with 5 calibration points minimum and minimum 75% of calibration standards to be within ± 20% of their nominal values. The main pharmacokinetic parameters were estimated by noncompartmental analysis (NCA) using Phoenix WinNonlin version 8.3.4 (Pharsight Corporation, USA). The pharmacokinetic parameters have been calculated from the mean value of plasma concentrations of GNE987P (**7**) analyte versus time profile after administration. The concentration of all pharmacokinetic samples that were calculated to be below the lower limit of quantitation (LLOQ) were considered as missing value (i.e. values for time points at 24h and longer for GNE987P (**7**) alone, or 360h and longer for either the PROxAb Shuttle complexed with GNE987P (**7**) or for the sequential administration of PROxAb Shuttle followed by GNE987P (**7**)) to better estimate $AUC_{0\text{-}inf}$, clearance and volume of distribution. The values for the terminal half-life ($t_{1/2}$) and the first order rate constant associated with the terminal log-linear portion of the curve (λz) were calculated only when at least 3 time points were quantifiable in the terminal phase of the linear regression. Values below the LLOQ were considered 0 ng/mL for descriptive statistics.

αEGFRxMIC7 complexed with GNE987 and GNE987 alone

The pharmacokinetic studies of αEGFRxMIC7 complexed with GNE987 (**6**) and of GNE987 (**6**) alone were performed at EMD Serono Research & Development Institute, Inc. Billerica and are described in the following. All parts of the study plan concerning animal care have been reviewed by the EMD Serono Billerica site "Institutional Animal Care and Use Committee (IACUC)" which reports to the EMD Serono Billerica site Head. Protection of animals used, housing and welfare are guaranteed according to the Protocol number 20-002: Pharmacokinetic Studies in Rodents, Principal Investigator: Mary-Jo Miller. Physical facilities for accommodation and care of animals are in accordance with the provisions of the AAALAC (Association for Assessment and Accreditation of Laboratory Animal Care) and the EMD Serono animal facility is recorded as AAALAC unit #001473. For GNE987 (**6**) alone, female C57BL/6N inbred mice (composite profile, n=9) provided from Taconic (NY, USA) received a single tail vein intravenous (i.v.) bolus injection of 0.30 mg/kg in 2% (v/v) DMSO/20% (v/v) (hydroxypropyl ß-cyclodextrin) Kleptose in water, at a dosing volume of 5 mL/kg. For the αEGFRxMIC7 PROxAb Shuttle complexed with GNE987 (**6**), C57BL/6N inbred mice (composite profile, n=9) provided from Taconic (NY, USA) received a single tail vein intravenous (i.v.) bolus injection of 30 mg/kg of the αCD33xMIC7 PROxAb Shuttle (corresponding to 0.38 mg/kg PROTAC) in 5% (v/v) DMSO in PBS, at a dosing volume of 5 mL/kg. For the free GNE987 (**6**), consecutive blood samples (25 µL) were taken sub-lingually under light isoflurane anesthesia (n=3 per group (G)) at 0.1 (G1), 0.5 (G2), 1 (G3), 2 (G1), 4 (G3), 6 (G2), and 24h (G3) on K3-EDTA in pre-chilled Eppendorf tubes, stored on ice for at least 15 min before centrifugation at 2500 x g for 10 min at 4°C to obtain plasma. For the αEGFRxMIC7 PROxAb Shuttle complexed with GNE987 (**6**), consecutive blood samples (25 µL) were taken sub-lingually under light isoflurane anesthesia (n=3 per group (G)) at 0.1 (G1), 2 (G2), 6 (G3), 24 h (G1), 72 (G2), 168 (G3), 240 (G1), 432 (G2), 600 (G3), 720 (G1) and 960h (G2) on K3-EDTA in pre-chilled Eppendorf tubes, stored on ice for at least 15 min before centrifugation at 2500 x g for 10 min at 4°C to obtain plasma. The sample preparation, analysis of the PROTAC and the estimation of pharmacokinetic parameters were the same as described above for αCD33xMIC7+GNE987P (**7**) and GNE987P (**7**), except that the PROTAC analyzed here is GNE987 (**6**) instead of GNE987P (**7**). The MRM transition for GNE987 (**6**) was 548.788 (m/z, z = 2) $\rightarrow$ 779.2 (m/z, z=1) and 329.101 (m/z, z=1) $\rightarrow$ 91 (m/z, z=1) for labetalol (IS). Also, the concentrations for the 720 and 960 h time points after the administration of the αEGFRxMIC7 PROxAb Shuttle complexed with GNE987 (**6**) were calculated to be below the lower limit of quantitation (LLOQ) and were considered as missing value for the estimation of $AUC_{0\text{-}inf}$, clearance and volume of distribution.

***In vivo* efficacy studies**

In vivo efficacy studies encompassing αCD33 PROxAb Shuttles were performed at Nuvisan ICB, Germany. Therefore, 3 million MV4-11 cells were injected subcutaneously in the left flank of untreated female CB17 SCID mice. Randomization of the animals in the different treatment groups and the initiation of the treatment was started after the average tumor size reached 150 mm^3. The control groups were treated with vehicle only (PBS pH 7.4, 5% DMSO (v:v)). The different groups were treated with 0.38 mg/kg GNE987 (**6**) and 30 mg/kg of either conjugated or unconjugated MIC7-based αCD33 PROxAb Shuttle (complexed with 0.38 mg/kg GNE987 (**6**)) once on day 1. Two additional groups were treated twice, either with 30 mg/kg of conjugated αCD33 PROxAb Shuttle (comprising 0.38 mg/kg GNE987 (**6**)) at day 1 followed by an additional treatment with 0.38 mg/kg GNE987 (**6**) at day 8 or with 0.38 mg/kg GNE987 at day 1 and 8. The individual groups were stopped before tumors reached a maximum tumor volume (1600 mm^3).

Supplementary Figures and Tables

Figures

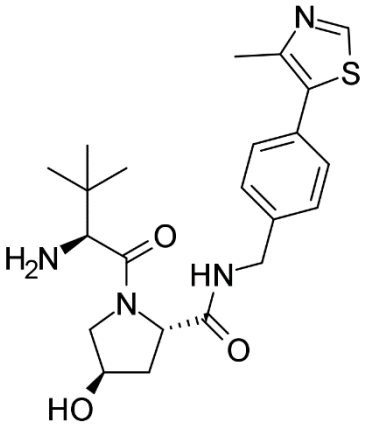

Figure S1. Structure of VHL Ligand VH032 (**5**).

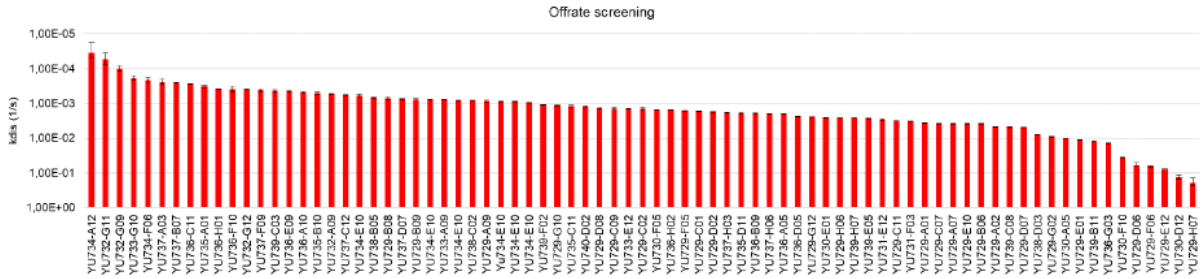

Figure S2. Off-rate screening using Bio-Layer Interferometry (BLI).The clones YU733-G10 and YU734-F06 refer to MIC5 and MIC7, respectively.

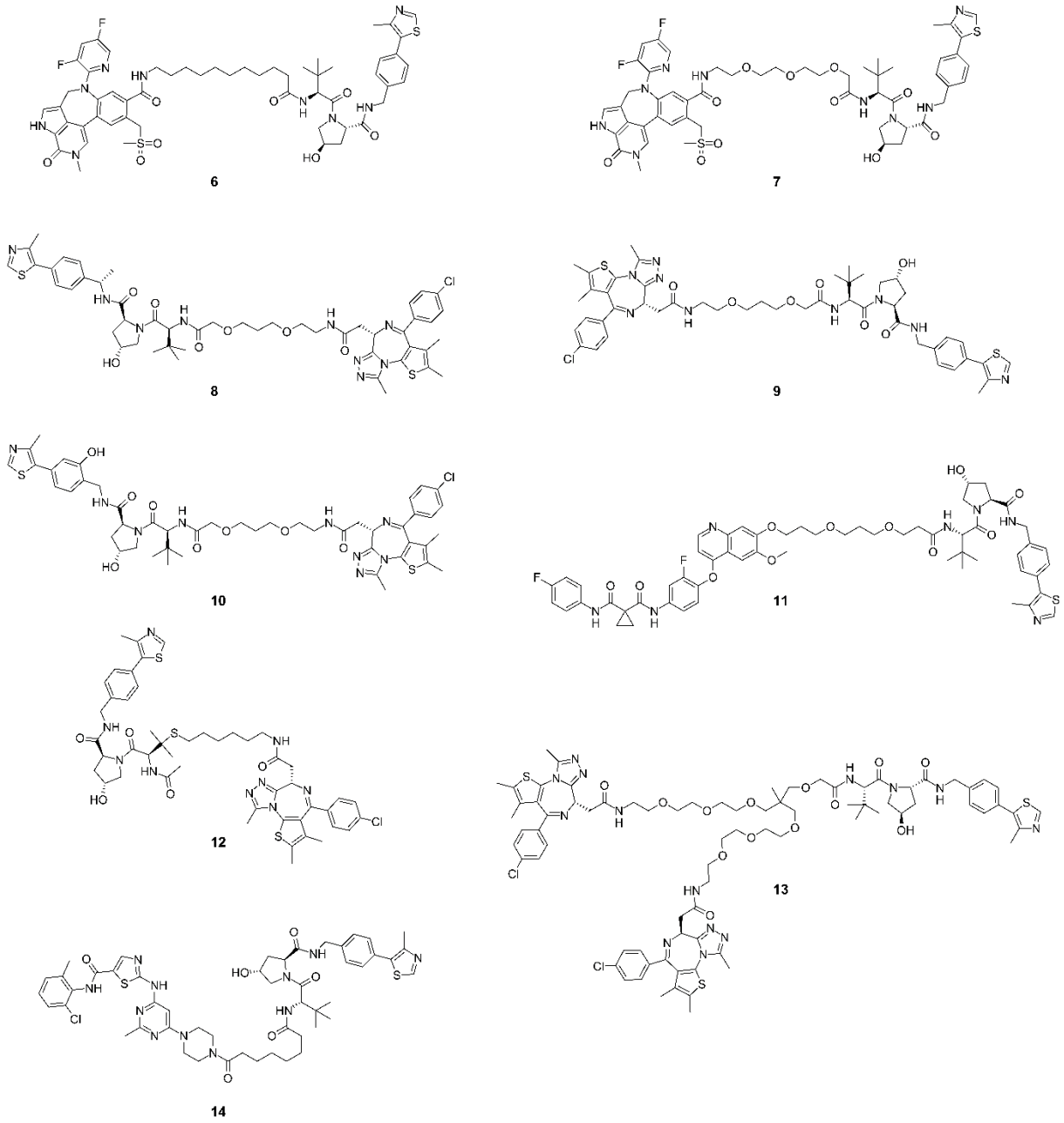

Figure S3. Structures of PROTACs used for SPR analytics: **6** (GNE987), **7** (GNE987P), **8** (ARV771), **9** (BETTY2), **10** (BETTY3), **11** (cMETd1); **12** (AT1), **13** (SIM1), and **14** (SIAIS178)

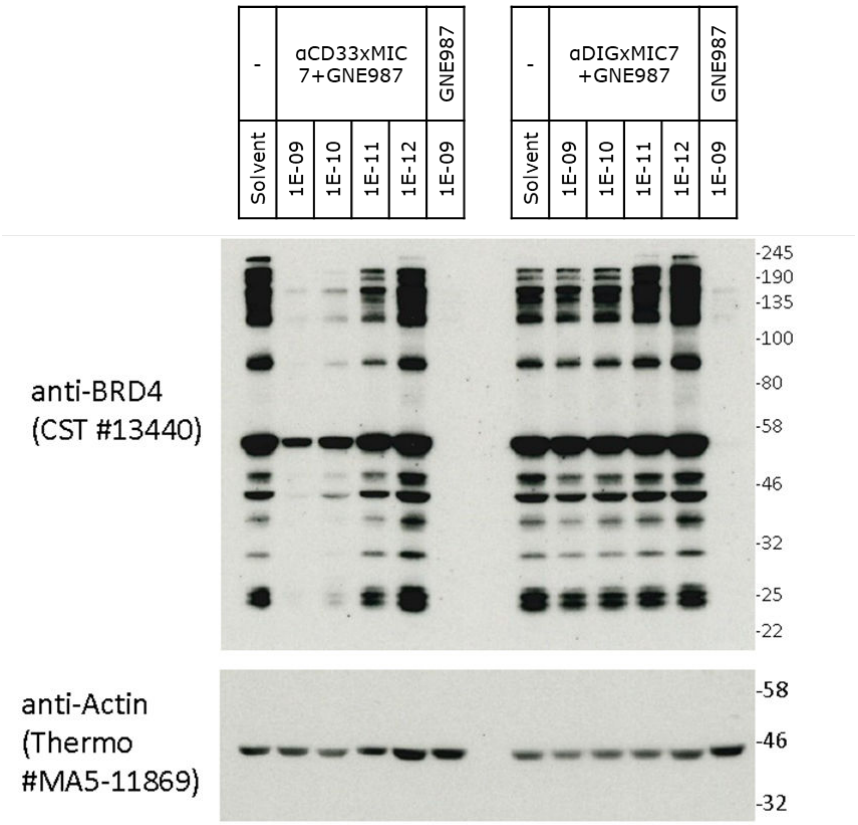

Figure S4. Western blot of MV4-11 cells treated with αCD33xMIC7 complexed with PROTAC GNE987 (**6**), negative control αDIGxMIC7+GNE987 (**6**) in serial dilution and PROTAC GNE987 (**6**) alone at 1 nM. All PROxAb Shuttles comprised a PROTAC-to-antibody ratio of 1:1.

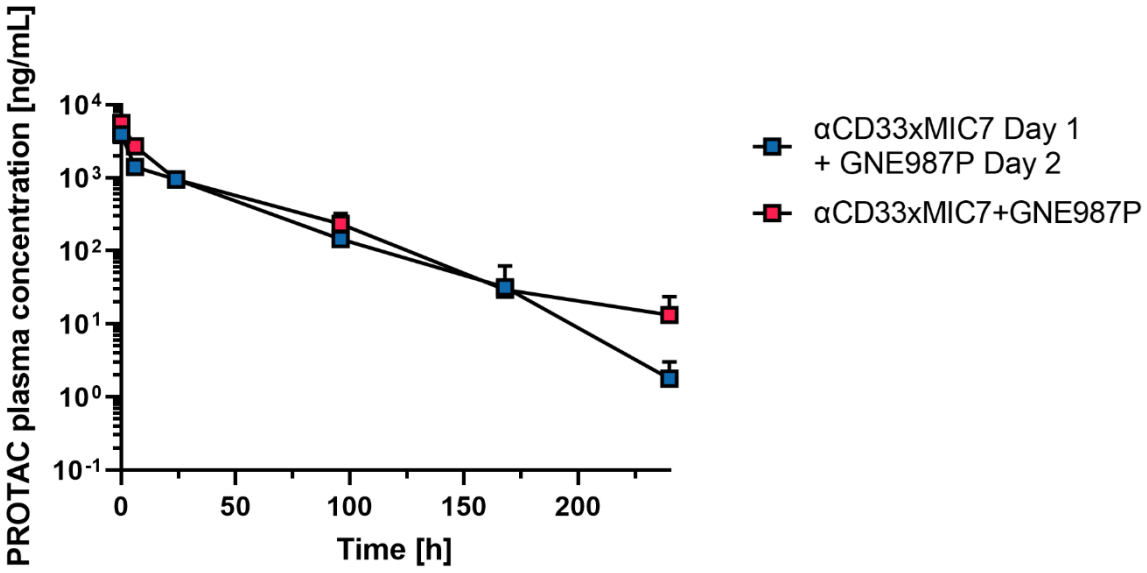

Figure S5. Pharmacokinetic analyses of total PROTAC. Total PROTAC profiles after administration of αCD33xMIC7 Shuttle after complexation with GNE987P (**7**) (red squares) and of sequentially administered non-complexed αCD33xMIC7 PROxAb Shuttle followed by administration of GNE987P (**7**) (blue squares) 24 hours later.

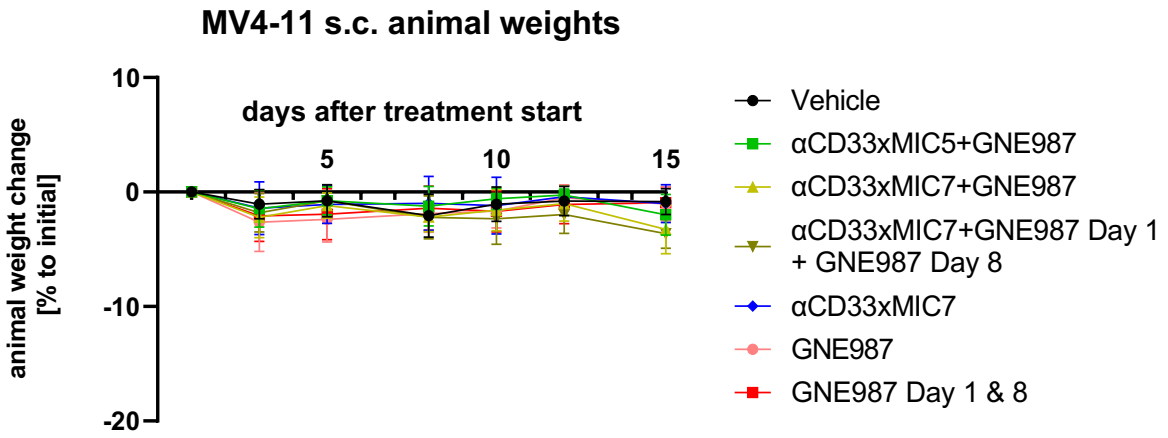

Figure S6. Animal Weights of MV4-11 tumor-bearing mice over time after indicated treatment.

Tables

Table S1. Affinity parameters of αCD33xMIC7 and αEGFRxMIC7 to different PROTACs from SPR measurements at 25 °C. N/D: not determined.

	αCD33xMIC7			αEGFRxMIC7		
PROTAC	**KD [M]**	**k_{on} [1/Ms]**	**k_{off} [1/s]**	**K_D [M]**	**k_{on} [1/Ms]**	**k_{off} [1/s]**
GNE987 (**6**)	4.19E-10	2.49E+05	1.01E-04	<1E-09	N/D	<1.00E-4
GNE987P (**7**)	1.96E-09	4.97E+05	9.23E-04	<1E-09	6.53E+05	3.20E-04
ARV771 (**8**)	1.07E-08	7.88E+05	3.92E-03	5.39E-09	1.39E+05	7.48E-04
BETTY2 (**9**)	2.11E-09	3.10E+05	6.50E-04	1.06E-09	3.15E+05	3.25E-04
BETTY3 (**10**)	3.26E-09	7.12E+05	2.31E-03	1.86E-09	3.77E+05	6.93E-04
cMETd1 (**11**)	1.23E-08	1.85E+04	2.28E-04	9.37E-09	1.85E+04	1.72E-04
AT1 (**12**)	2.07E-09	1.08E+06	2.23E-03	1.20E-09	2.95E+05	3.55E-04
SIM1 (**13**)	4.76E-09	1.54E+05	9.27E-04	1.90E-09	6.71E+04	1.27E-04
SIAIS178 (**14**)	8.31E-09	1.14E+04	9.50E-05	<1E-09	N/D	<1.00E-4

Table S2. Potencies of PROxAb Shuttles targeting different tumor associated antigens (TAA) (αCD33xMIC7 or αEGFRxMIC7, respectively) complexed with GNE987 (**6**) or GNE987P (**7**) (PROTAC-to-antibody ratio of 1:1) and free PROTAC GNE987 (**6**) or GNE987P (**7**) on CD33-positive and EGFR-positive cells as well as respective negative cell lines (RAMOS for CD33 and HEPG2 for EGFR). N/T: not tested.

Cell line	TAA	αTAAxMIC7 + GNE987	αDIGxMIC7+ GNE987	GNE987 (6)	αTAAxMIC7+ GNE987P	αDIGxMIC7+ GNE987P	GNE987P
MV411	CD33	0.28 nM	8.1 nM	< 0.03 nM	0.059 nM	35 nM	0.26 nM
MOLM13	CD33	8.1 nM	>100 nM	0.020 nM	6.9 nM	>100 nM	3.7 nM

RAMOS	CD33	>100 nM	>100 nM	0.089 nM	>100 nM	>100 nM	15 nM
A431	EGFR	0.26 nM	>100 nM	0.25 nM	N/T	N/T	N/T
MDAMB468	EGFR	0.27 nM	>100 nM	0.16 nM	N/T	N/T	N/T
HEPG2	EGFR	>100 nM	>100 nM	2.2 nM	N/T	N/T	N/T

Table S3. IC50 values of PROxAb Shuttles targeting various tumor-associated antigens such as HER2, BCMA, NAPI2B and EGFR complexed with PROTACs GNE987 (**6**), GNE987P (**7**) or SIM1 (**13**) on receptor-positive cell lines. The PROTAC-to-antibody ratio (PAR) was adjusted according to the PAR column.

Cell line	Target	PROxAb Shuttle clone	PROTAC	IC50 [M] PROTAC	IC50 [M] αTAAxMIC7	IC50 [M] αDIGxMIC7	PAR	Antibody Isotype
BT474	HER2	MIC7	GNE987	7.5E-11	1.5E-10	1.7E-08	1.0	IgG1-PG-LALA
BT474	HER2	MIC7	GNE987P	2.6E-09	2.0E-10	3.5E-08	1.0	IgG1-PG-LALA
MDAMB453	HER2	MIC7	GNE987	9.4E-11	8.7E-11	4.5E-08	1.0	IgG1-PG-LALA
MDAMB453	HER2	MIC7	GNE987P	4.4E-09	5.2E-10	3.0E-08	1.0	IgG1-PG-LALA
SKBR3	HER2	MIC7	GNE987	1.5E-10	1.9E-10	2.1E-09	1.0	IgG1-PG-LALA
SKBR3	HER2	MIC7	GNE987P	1.5E-08	2.1E-10	5.3E-08	1.0	IgG1-PG-LALA
K562	BCMA	MIC7	GNE987	2.0E-10	1.9E-07	2.9E-08	1.0	IgG1-PG-LALA
K562	BCMA	MIC7	GNE987P	2.8E-08	> 1.0E-07	> 1.0E-07	1.0	IgG1-PG-LALA
LP1	BCMA	MIC7	GNE987	7.8E-11	3.4E-08	> 1.0E-07	1.0	IgG1-PG-LALA
LP1	BCMA	MIC7	GNE987P	4.7E-09	3.4E-08	> 1.0E-07	1.0	IgG1-PG-LALA
NCIH929	BCMA	MIC7	GNE987	1.3E-11	2.0E-10	3.2E-08	1.0	IgG1-PG-LALA
NCIH929	BCMA	MIC7	GNE987P	5.6E-10	9.1E-11	2.8E-08	1.0	IgG1-PG-LALA
OPM2	BCMA	MIC7	GNE987	< 3.0E-11	3.6E-09	5.1E-08	1.0	IgG1-PG-LALA
OPM2	BCMA	MIC7	GNE987P	4.8E-10	9.9E-10	3.8E-08	1.0	IgG1-PG-LALA
OVCAR3	NAPi2B	MIC7	GNE987	2.9E-10	2.8E-10	> 1.0E-07	1.0	IgG1-PG-LALA
MOLM13	B7H3	MIC7	GNE987	1.9E-10	4.0E-10	4.6E-08	1.5	IgG4-PG-SPLE
MOLM13	B7H3	MIC7	GNE987P	5.8E-09	1.5E-07	N/T	1.5	IgG4-PG-SPLE
MV411	B7H3	MIC7	GNE987	4.7E-11	9.0E-11	1.2E-08	1.5	IgG4-PG-SPLE
MV411	B7H3	MIC7	GNE987P	4.0E-10	2.4E-09	N/T	1.5	IgG4-PG-SPLE

U937	B7H3	MIC7	GNE987	2.3E-10	3.9E-10	1.0E-07	1.5	IgG4-PG-SPLE
U937	B7H3	MIC7	GNE987P	1.5E-09	3.2E-08	N/T	1.5	IgG4-PG-SPLE
MOLM13	CLL1	MIC7	GNE987	5.4E-11	4.4E-08	> 1.0E-07	1.5	IgG4-PG-SPLE
MOLM13	CLL1	MIC7	GNE987P	3.6E-09	3.5E-08	> 1.0E-07	1.5	IgG4-PG-SPLE
U937	CLL1	MIC7	GNE987	1.2E-10	6.0E-08	> 1.0E-07	1.5	IgG4-PG-SPLE
U937	CLL1	MIC7	GNE987P	2.1E-09	2.3E-08	> 1.0E-07	1.5	IgG4-PG-SPLE
K562	CLL1-negative	MIC7	GNE987	3.7E-10	> 1.0E-07	> 1.0E-07	1.5	IgG4-PG-SPLE
K562	CLL1-negative	MIC7	GNE987P	4.2E-08	> 1.0E-07	> 1.0E-07	1.5	IgG4-PG-SPLE
A431	EGFR	MIC7	GNE987P	1.6E-07	5.6E-10	> 1.0E-07	1.0	IgG1-PG-LALA
A431	EGFR	MIC7	SIM1	3.5E-09	5.5E-10	> 1.0E-07	1.0	IgG1-PG-LALA
MDAMB468	EGFR	MIC7	GNE987P	4.6E-08	6.8E-10	> 1.0E-07	1.0	IgG1-PG-LALA
MDAMB468	EGFR	MIC7	SIM1	5.7E-09	8.1E-10	> 1.0E-07	1.0	IgG1-PG-LALA
MV411	CD33	MIC5	GNE987P	5.2E-10	1.3E-10	-	0.5	IgG4-PG-SPLE
MV411	CD33	MIC5	GNE987P	5.2E-10	1.1E-10	-	1.0	IgG4-PG-SPLE
MV411	CD33	MIC5	GNE987P	5.2E-10	8.2E-12	-	1.5	IgG4-PG-SPLE
MV411	CD33	MIC5	GNE987	9.0E-12	3.2E-11	-	1.0	IgG4-PG-SPLE
MOLM13	CD33	MIC5	GNE987	4.7E-11	4.4E-09	-	1.0	IgG4-PG-SPLE

Table S4. SPR affinity data for αCD33xMIC5 and αCD33xMIC7 binding to GNE987 (**6**) or GNE987P (**7**) at 37 °C.

PROTAC	**αCD33xMIC5**			**αCD33xMIC7**		
	k_{on} (1/Ms)	**k_{off} (1/s)**	**K_D (M)**	**k_{on} (1/Ms)**	**k_{off} (1/s)**	**K_D (M)**
6 (GNE987)	3.84E+05	2.19E-03	5.70E-09	2.49E+05	1.04E-04	4.19E-10
7 (GNE987P)	-	-	-	2.70E+05	8.1E-04	2.98E-09

Table S5. Affinities (K_D), change in enthalpy (ΔH) and stoichiometry (N) of wildtype αCD33xMIC7 and humanized variants αCD33xMIC7_1.1-MIC7_1.6 when binding to VH032 derived from isothermal calorimetry measurements.

Clone	Backbone	K_D [nM]	ΔH [kJ mol^{-1}]	N
αCD33xhMIC7_1.6	IgG1 PG-LALA	<1	-71	2.0
αCD33xhMIC7_1.5	IgG1 PG-LALA	<1	-80	2.0
αCD33xhMIC7_1.4	IgG1 PG-LALA	~3	-69	2.1
αCD33xhMIC7_1.3	IgG1 PG-LALA	<1	-69	2.0
αCD33xhMIC7_1.2	IgG1 PG-LALA	<2	-61	2.0
αCD33xhMIC7_1.1	IgG1 PG-LALA	<1	-49	2.1
αCD33xMIC7_1.0	IgG1 PG-LALA	<1	-57	1.8
αCD33xMIC7	IgG4 PG-SPLE	5	-52	2,1

Table S6. Affinity parameters of humanized αCD33xhMIC7_1.6 binding to PROTAC GNE987 (**6**) and GNE987P (**7**) derived from SPR measurements at 25 °C.

Name	k_{on} [1/M]	k_{off} [1/s]	K_D [1/Ms]
6 (GNE987)	3.2E+04	3.9E-05	1.2E-09
7 (GNE987P)	2.6E+05	2.2E-04	8.6E-10

Ethical statement

In vivo studies were either performed at Istituto di Ricerche Biomediche “Antoine Marxer” – RBM Colleretto Giacosa (TO), Italy, Nuvisan ICB GmbH, Berlin, Germany or EMD Serono Research & Development Institute, Inc. Billerica, MA 01821, USA. At at Istituto di Ricerche Biomediche “Antoine Marxer” – RBM Colleretto Giacosa all parts of the studies concerning animal care have been either reviewed by the RBM Designed Veterinarian and Animal Welfare Officer. Protection of animals used, housing and welfare are guaranteed according to the Italian D.Lvo No. 26 of March 4, 2014. Physical facilities for accommodation and care of animals are in accordance with the provisions of the Italian D.Lvo 2014/26 and of Directive 2010/63/EU. The Institute is fully authorized by Italian Ministry of Health. For studies performed at Nuvisan ICB, Berlin all animal experiments were approved by the local ethics committee on animal research (Landesamt für Gesundheit und Soziales Berlin, Bereich des Veterinärwesens, Germany, LaGeSo No. G 0200/19). At EMD Serono Research & Development Institute, Inc. Billerica all parts of the study plan concerning animal care have been reviewed by the EMD Serono Billerica site “Institutional Animal Care and Use Committee (IACUC)” which reports to the EMD Serono Billerica site Head. Protection of animals used, housing and welfare are guaranteed according to the Protocol number 20-002: Pharmacokinetic Studies in Rodents, Principal Investigator: Mary-Jo Miller. Physical facilities for accommodation and care of animals are in accordance with the provisions of the AAALAC (Association for Assessment and Accreditation of Laboratory Animal Care) and the EMD Serono animal facility is recorded as AAALAC unit #001473.

Livestock farming and immunization of New World Camelids (llamas, alpacas, huarizos) was managed by preclinics GmbH according to the relevant national and international guidelines. The study was approved by an Institutional Animal Care and Use Committee, the Lower Saxony State Office for

consumer protection and food safety (Oldenburg, Germany, reference number 33.19-42502-05-17A210).

References

[1] Q. Zhao, C. Ren, L. Liu, J. Chen, Y. Shao, N. Sun, R. Sun, Y. Kong, X. Ding, X. Zhang, Y. Xu, B. Yang, Q. Yin, X. Yang, B. Jiang, *J. Med. Chem.* **2019**, *62*, 9281–9298.

[2] Y. Shen, G. Gao, X. Yu, H. Kim, L. Wang, L. Xie, M. Schwarz, X. Chen, E. Guccione, J. Liu, M. T. Bedford, J. Jin, *J. Med. Chem.* **2020**, *63*, 9977–9989.

[3] T. Schlothauer, S. Herter, C. F. Koller, S. Grau-Richards, V. Steinhart, C. Spick, M. Kubbies, C. Klein, P. Umaña, E. Mössner, *Protein Eng. Des. Sel.* **2016**, *29*, 457–466.